GETTERING IN SILICON

Transition metals in silicon have been a constant problem in the integrated circuit (IC) industry. They are generally fast diffusers with high solubilities (1) at high temperatures. The most common metal contaminants, Cr, Fe, Cu, and Ni, can easily be introduced from stainless steel and copper processing equipment. Introduction of the metals into the wafer happens during ingot growth, from cleaning solutions, etching acids, or ion implants, or directly from the furnace during a high-temperature anneal. Even at low concentrations (1×10^{12} at./cm^3), transition metals can reduce the device yield. The metal contamination exhibits various deleterious effects depending upon the device.

- *pn Diodes.* When dissolved in silicon, transition metals can form deep levels (2), which act to degrade device performance by the generation (3) (or recombination in small forward biases) of carriers in any reverse-biased depletion regions. Impurities can lower the reverse bias breakdown voltage (4) and increase leakage currents (5,6). Metal precipitates can also form bands of deep levels (7,8) and short *pn* junctions (9,10).
- *Bipolar Devices.* Dissolved metals in bipolar junction transistors (BJT) generally increase the base currents, degrading the emitter efficiency and base transport factors (3). The net result is an increase in parasitic currents, power consumption, and heat production. While such effects may in some cases be tolerated, more debilitating are the effects of metal precipitates, which can cause emitter–collector shorts (9–11).
- *MOS Devices.* MOS devices are most sensitive to imperfections in the oxide layer and the Si–SiO_2 interface (12). Unfortunately, studies demonstrate that many transition metals segregate to or precipitate at the Si–SiO_2 interface, or they become trapped in the oxide layer itself (13,14). The net result is a breakdown in the dielectric strength of thin oxide layers (15–23) and/or an increase in generation rates (24). Transition metals have thus been linked to poor retention times (high refresh rates) in dynamic random access memories (25).
- *Charge-Coupled Devices (CCDs).* CCDs are extremely sensitive to contamination by metals, since they often form deep-level traps. The generation current from such traps is a source of noise and can, if large enough, cause pixel failures. Iron levels in such devices are on average 5.4×10^8 Fe_i/cm^3 (0.015 interstitial Fe atom/pixel) and gold levels 3.6×10^8 Au/cm^3 (0.01 Au atom/pixel) (26).
- *Photovoltaics (PVs).* Solar cell collection efficiency is degraded by recombination centers. These centers can be due to dissolved or precipitated metal impurities introduced during growth and/or processing. It is a continuing challenge to passivate and/or getter these defects without introducing costly processing steps (27–34).
- *Enhanced Structural Defect Formation.* Dissolved metals have been shown to decrease the barrier of formation for defects such as oxidation-induced stacking faults (OSF) and dislocations (35). Iron has also been shown to enhance the nucleation and growth of oxygen precipitates (36). These effects may help induce deleterious structural

defects in device regions, which have been observed in failed devices (10,37).

Gettering techniques keep unintentionally introduced metals away from the device regions. The actual criteria for successful gettering varies depending upon the application. From the materials science point of view, these criteria break down as follows:

- *ICs.* Prevention of surface precipitation (haze) and near-surface defects, including metal-induced defects
- *CCDs.* additional reduction of dissolved metals in the near-surface region
- *PVs.* removal of dissolved and precipitated metals from bulk

These techniques are not only insurance against accidental contamination, but also necessary to maintain high yields. The current gettering techniques have been optimized primarily through yield studies, and, while little is known of the quantitative aspects, the techniques appear adequate for current fabrication technologies. However, the IC industry is quickly moving toward larger wafers (38) (possibly with lower oxygen concentrations), novel structures (SOI, silicon on insulator, epitaxial layers, etc.), highly doped substrates (power devices), back-side treatments (polysilicon (39) deposition or polished back sides), rapid thermal anneal (RTA) processes, smaller device dimensions, and larger electric fields and current densities (40,41). This imposes increasingly strict requirements on the reduction of impurities in silicon substrates. The Semiconductor Industry Association (SIA) guidelines for metal concentrations in incoming wafer are $\leq 10^{10}$ at./cm^3 for 1998 to 2000 (38). It is unlikely that these levels can be maintained solely through preventative measures, such as higher-purity chemicals, cleaner furnaces, and general improvements to the processing conditions. Tremendous effort is spent on preventive techniques, yet the yield is becoming ever more sensitive to the slightest perturbations of the manufacturing environment. Thus it is imperative to understand not only the mechanisms of gettering, but also its quantitative aspects, which can be used in predictive computer simulations to optimize gettering processes.

A BRIEF OVERVIEW OF GETTERING

In general, gettering is a three-step process (42). The impurity must be (1) released from its original and undesirable state so that it can then (2) diffuse through the crystal and be (3) captured at the gettering site. The release process has only recently begun to be studied. Initial results from McHugo et al. (43) have demonstrated the rapid release of Cu and Ni from dislocations in polycrystalline silicon, indicating that release is rapid with no observable barrier. For the slower-diffusing transition metals such as iron, diffusion to the gettering site is typically the rate-limiting step. There are two general classes of gettering processes, defined by their capture mechanisms: segregation and relaxation (44).

Synopsis of Relaxation Gettering

In any relaxation gettering technique, heterogeneous precipitation sites are intentionally formed in regions away from the device/surface region. The gettering process occurs with an impurity supersaturation which can occur during cooling from high temperatures. Any mobile and supersaturated impurities can quickly precipitate only in regions of the silicon wafer that contain high concentrations of precipitation sites. In these regions, the dissolved impurity concentration will decrease rapidly and might not deviate significantly from the thermodynamic equilibrium concentration. In neighboring regions, such as the device/surface region with low nucleation site densities, supersaturated impurities cannot precipitate quickly, and thus impurity concentrations may significantly exceed the thermodynamic equilibrium concentrations during cooling. This difference in precipitation site density creates a dissolved-impurity concentration gradient. In this manner, supersaturated impurities diffuse away from the surface/device region and into the bulk during a cooldown. This process is referred to as relaxation gettering because it requires the supersaturation of impurities to *relax* to equilibrium concentrations during a cooling step. There are two types of relaxation gettering techniques: internal and back-side gettering.

Internal gettering is also called intrinsic gettering, since the gettering defects are viewed as inherent in the Czochralski (Cz) wafer. Internal gettering has been used widely in industry by utilizing oxygen precipitates and associated structural defects as heterogeneous nucleation sites for any supersaturated transition metals. There had been a debate over the years as to which particular defect was responsible for gettering. Presently, it is recognized that different impurities will nucleate on different defects. Furthermore, it is understood that the cooling rate has a significant effect on which sites are nucleated and on the overall gettering efficiency.

Back-side relaxation gettering typically involves heterogeneous nucleation sites formed by damaging the back side of the wafer or by depositing a layer of polysilicon that itself contains many heterogeneous nucleation sites such as dislocations and grain boundaries. Back-side gettering techniques are effective for fast diffusing impurities such as copper and nickel.

Synopsis of Segregation Gettering

Segregation gettering utilizes a region of higher impurity solubility to extricate impurities from a region of lower solubility. The segregation gettering layer is located outside of the active device region and has the advantage over relaxation gettering that no supersaturation is required. Thus, in principle, low impurity concentrations in the device region can be realized quickly at a temperature where the impurities can diffuse quickly. A *segregation coefficient* is defined as the ratio of the impurity solubility in the gettering region to that in the device region. Segregation can result from various conditions:

- *Phase.* Liquid silicon has a much higher solubility for transition metals than crystalline silicon. This is widely exploited during Cz growth of Si ingots.
- *Material.* Other boundary materials, such as aluminum, have greater transition metal solubilities than crystalline silicon, simply due to their different chemical composition.
- *Fermi Level.* Manipulation of the Fermi level in a gettering region can increase the ratio (dynamic equilibrium) between the dissolved ionized and neutral metal impu-

rity (45–48). Thus the gettering region will contain a larger total dissolved metal concentration.

- *Traps.* Pairing reactions, (46,49–51) between dopants and several transition metals can also increase the total metal concentration in highly doped materials.
- *Strain.* Strain has also been thought to increase (or decrease) the solubility of transition metals and has been demonstrated to either getter metals directly (52,53) or influence metal gettering at defects (54).

For IC devices in silicon, with the active device region within 1 μm of the front surface of the substrate, the gettering layer is typically placed in the proximity of the front surface (>1 μm depth) or at the rear surface of the substrate. Alternatively, the active device region of a silicon photovoltaic cell is the entire substrate thickness, so segregation gettering to the front or back surface is appropriate.

Segregation gettering of impurities in a semiconductor can be accomplished by numerous methods. For photovoltaic silicon substrates, the most commonly used methods are aluminum and phosphorus gettering. Epitaxial films grown on high quality substrates are becoming of great importance to the IC industry. One of the structures that are of particular interest is a p epitaxial layer grown on a p^{++} substrate (p/p^{++}). Aside from device design advantages, there exists the added advantage that Fermi level and/or trapping segregation between the p layer and the p^{++} substrate can reduce transition metal contaminant concentration in the p layer to extremely low levels. Increased solubility due to the Fermi effect is discussed by Hall and Racette (55), Gilles et al. (56), Stolk et al. (57), and McHugo et al. (58).

Trends

In the past the IC industry has relied primarily on internal relaxation gettering. Future gettering techniques will most likely include some type of segregation gettering as well, since relaxation gettering alone may no longer be able to achieve the necessary reduction in metal concentrations in the lower thermal budgets, which are required for very shallow junctions. In principle, segregation techniques have the advantage of being effective even when the impurity is not supersaturated.

DEFINITION OF SOLUBILITY

A clear understanding of solubility is important in both segregation and relaxation gettering, since segregation relies on a difference in solubility between two regions and relaxation relies on a difference in solubility from equilibrium values. Solubilities of transition metals in silicon are defined as the equilibrium dissolved metal concentration in silicon when bounded by a specific phase (1). For example, the solubility of interstitial iron in silicon (below eutectic) is defined as the equilibrium concentration of iron when $FeSi_2$ is the unstressed boundary phase on the surface. If the boundary phase were FeSi, or pure Fe, a different solubility would be obtained. Indeed, such an effect was observed by Weber (1). Since time is required for the $FeSi_2$ phase to establish itself at the surface after deposition of pure Fe, the solubilities measured by Weber at short times were different than the final equilibrium concentrations.

The familiar thermodynamic expression for solubility is,

$$C^{eq} = e^{-\Delta G/kT} = e^{\Delta S/k} e^{-\Delta H/kT} = C_0 e^{-\Delta H/kT} \tag{1}$$

where ΔH, ΔS, and ΔG are the enthalpy, entropy, and free energy of formation, respectively. The energy of formation ΔG is actually the sum of a number of energy terms as,

$$\Delta G = E_b - E_e + E_s \tag{2}$$

where E_b is the binding energy of the metal to the boundary phase, E_e is the electron interaction energy, and E_s is the strain energy.

Microscopically, a metal atom must detach itself from the surface silicide before it can enter the silicon. This is a thermally activated process, and the energy required for the detachment is essentially a binding energy E_b, which in fact determines the vapor pressure of the metal over the silicide. Assuming for the moment the absence of other effects, the solubility of a metal in silicon should therefore be equivalent to the vapor pressure of the metal over the silicide (or other boundary material) (59). It is immediately clear, for example, that Fe, FeSi, and $FeSi_2$ all have different binding energies for iron, resulting in different vapor pressures, and therefore different solubilities in silicon. There are additional interactions between the silicon matrix and the metal impurity. These interactions result from:

- the interaction of the outer electron orbitals of the metal and the silicon matrix, E_e
- the elastic strain energy of an impurity, E_s

Clearly the electron interaction can be significant, since a number of metals can be ionized much more easily as an interstitial in silicon than as a single atom in a vacuum. For most of the 3d transition metals, except Ti and Cr, the metallic radius is small enough to fit into the tetrahedral site without producing any elastic strain (60).

From this rough examination of solubility, it stands to reason that a change in the silicon matrix due to strain, structural defects, or melting will affect one or both of the interaction energies. Masuda-Jindo (61) attempted to calculate the interaction (segregation) energy between strained regions resulting from structural defects and metal impurities [i.e. E_e(defect) $-$ E_e(matrix)] using linear combination of atomic orbitals (LCAO). His results indicated that the transition metals V, Cr, Mn, Fe are attracted to tensile regions ($E_{seg} \approx$ 0.25 eV for 5% tensile strain), while Cu is attracted to compressed regions. Certainly these trends need to be verified experimentally, but the general conclusion is that structural changes will most likely affect the equilibrium concentration (solubility) of metal impurities. One can, in fact, view the defect structure (i.e. the dislocation core) as a different phase with a different solubility. However, judging from the above results, very large strains may be required to obtain only weak segregation.

Additionally, metal impurities may be ionized and then paired. Since only the neutral species is in equilibrium with the boundary phase silicide, the additional ionized and paired species increase the total amount of metal present in the sili-

con. The entire reaction can be described as,

$$M_{\text{silicide}} \leftrightarrow M^0 \leftrightarrow M^{+,-} \leftrightarrow M^+A^- \text{ or } M^-D^+ \quad (3)$$

Since the term *solubility* is used to indicate the total metal concentrations, ionization and pairing increase the solubility of the metal in the silicon. Further discussion of solubility will be presented in relevant portions of the text.

RELAXATION GETTERING

Historical Aspects

One of the earliest studies on relaxation gettering was by Kaiser (62) who in 1957 proposed a complexing reaction between intentionally grown oxygen precipitates and metal impurities. Mets (63) in 1965 elaborated on the possible complexing and/or precipitation of copper and regions with high oxygen concentrations. Furthermore, he clearly demonstrated the gettering of copper by damaged surfaces. Twelve years later, in 1977, Tan et al. (64) presented the first comprehensive model of internal relaxation gettering with an intentionally formed denuded zone and bulk heterogeneous nucleation sites. Additionally, they demonstrated yield improvement by using this method.

In numerous early works on gettering, the exact capture process was not always explicitly specified. Discerning segregation from relaxation effects in internal, back-side damage or polycrystalline back-side gettering experiments is not always straightforward, especially when monitoring-device yields or etchpit densities are used as indications of gettering. Copper and other metals were often said to be "trapped" and "gettered" by dislocations or oxygen precipitates (65–67), leaving the exact gettering mechanism ambiguous. Involvement of silicon interstitials was often speculated. Much progress in understanding relaxation gettering has been made since the early studies. The next section on the kinetics of relaxation gettering will explain the mechanism of relaxation gettering by describing the precipitation rate and the diffusion of impurities. The following section will discuss the details of heterogeneous precipitation sites. Two of the primary relaxation methods, internal and back-side gettering, will be discussed at the end of this section.

General Mechanism

Kinetics of Relaxation Gettering. A fundamental aspect of relaxation gettering is the difference in the precipitation rate of an impurity in the device and gettering regions. To first order, this difference depends upon the density of precipitation sites, that is, successfully nucleated defects. A computer simulation of a slow cool process with an initial dissolved iron concentration of 3×10^{13} Fe/cm^3 is shown in Fig. 1. The cool begins at 850°C and ends at 200°C with a slow rate of 80°C/min. As time increases, the equilibrium solubility (1) decreases and is shown by the heavy dashed line in Fig. 1. Since diffusion takes time, the more precipitation sites there are, the sooner an impurity can precipitate. In Fig. 1, the iron precipitation sites are assumed to correlate directly with an oxygen precipitate density, implying that iron has nucleated at the oxygen precipitates.

To illustrate such a concentration gradient, a computer simulation was performed simulating relaxation gettering of

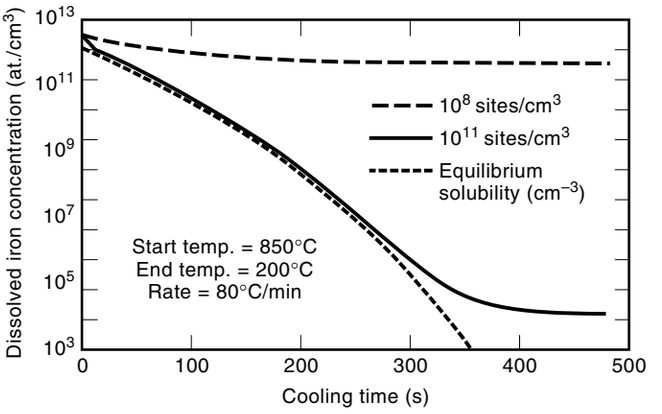

Figure 1. Illustration of precipitation during a slow cool. During the cool from 850°C to 200°C, the equilibrium solubility (1) of the iron decreases as shown by the dotted line. Dissolved iron can precipitate quickly if a large number of precipitation sites are available as shown by the solid line. If few precipitation sites are available, precipitation of iron is reduced as shown by the dashed line.

a 40 μm epitaxial layer on a substrate with a large concentration of oxygen precipitates and is shown in Fig. 2. During the slow cool, dissolved iron in the epitaxial layer precipitates very slowly, since it is assumed that the density of precipitation sites in the epitaxial layer is very small. In the bulk region, there is a high density of precipitation sites and iron precipitates rapidly. The dotted curve labeled "Dissolved" in Fig. 2 is the concentration profile of dissolved iron at the end of cooling. It clearly shows a concentration gradient and thus a flux of iron out of the epitaxial layer and into the bulk where it precipitates. The flux of iron due to the concentration gradient is established once the iron begins to precipitate in the bulk, and continues until the diffusivity of iron becomes so low that diffusion out of the epitaxial layer becomes insignificant. The total iron concentration, dissolved and precipitated, at the end of the slow cool is also shown in Fig. 2. One

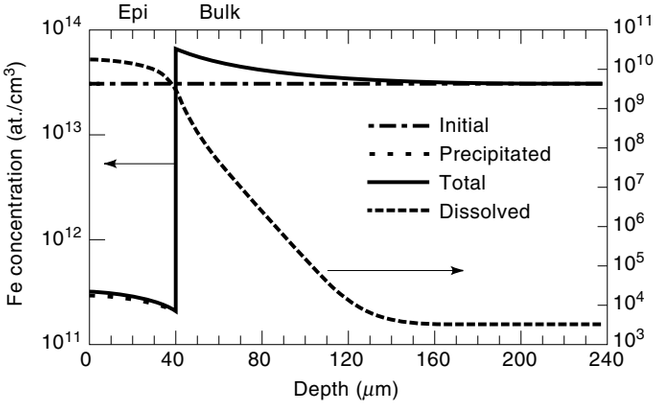

Figure 2. Illustration of the dissolved iron concentration gradient during a slow cool. In the bulk there is a high density of precipitation sites and iron precipitates quickly. In the epitaxial layer there are few precipitation sites and the dissolved iron does not significantly precipitate. This results in a concentration gradient and therefore a flux of iron from the epitaxial layer to the bulk, as is shown by the "Dissolved" line.

can clearly see that the total iron concentration in the epitaxial layer has dropped by approximately two orders of magnitude.

While the qualitative picture of relaxation gettering is straightforward, the quantitative aspects are more difficult and may be why a complete understanding of relaxation gettering has languished for so long. The difficulties in quantifying relaxation gettering include the following:

Metal impurities have different precipitation behavior, as will be discussed later.

The cooling rate affects the number of heterogeneous sites that are actually nucleated.

Direct characterization methods, such as transmission electron microscopy (TEM), cannot be used to determine an overall effective nucleation site density and gettering efficiency.

It is clear that in order to quantify relaxation gettering, one must quantify the precipitation rate from a macroscopic standpoint.

Earlier, it was stated that to first order, the precipitation rate (the rate at which the solute disappears, not the rate at which precipitates are formed) is proportional to the density of precipitation sites. To be more exact, the time constant of a purely diffusion limited precipitation process is proportional to the product of the density of precipitation sites, n, and the radius of the precipitation sites, r_0. This follows from the analytic solutions for the average solute concentration during precipitation, which were derived by Ham (68) in 1958. He presented two solutions for precipitation onto spherical precipitates: one solution assumes a growing precipitate, and the other a nongrowing precipitate. Using these solutions, the rate of precipitation can be quantified. However, there are several assumptions used in deriving these solutions:

- The nucleation site density n is constant. This may be the case in heterogeneous nucleation or in homogeneous nucleation where there is a distinct nucleation and then a growth stage. Ham's results would apply only to the growth stage.
- The process is diffusion-limited only. Nucleation-limited precipitation and reaction-limited precipitation are not considered.
- The nucleation site distribution is random.
- The initial solute concentration is uniform and can be adequately described by an average concentration $\bar{c}_0$.
- The radius of the precipitate, r_0, is much smaller than the distance between precipitates, r_s.

Whether all of these conditions are met during precipitation of transition metals in silicon is uncertain. The manner in which copper precipitates on dislocations may preclude any quantitative analysis based on Ham's equations. This will be discussed later.

To simplify the problem, Ham solved Fick's diffusion equation assuming a fixed precipitate radius rather than a growing radius. For a precipitate of fixed radius, Ham finds that the precipitation process is adequately described by

$$\bar{c}(t) - c_s \approx (c_0 - c_s)e^{-t/\tau_0} \tag{4}$$

where

$$\tau_0 = \frac{1}{4\pi n r_0 D} \tag{5}$$

and r_0 is the fixed precipitate radius.

Ham also showed that when the radius does not change significantly (i.e., when more than 50% of the solute has precipitated), the growing-radius solution then approximates the fixed-radius solution as

$$\frac{\bar{c}(t) - c_s}{c_0 - c_s} \approx ke^{-t/\tau_0} \tag{6}$$

where k is a constant that is larger than 1 and depends on the ratio n/c_0, and τ_0 is given in Eq. (5). In this case, r_0 is taken as the radius of the precipitate when more than 50% of the impurity has precipitated. This is due to the fact that the radius increases as the cube root of the volume. Once approximately half the solute has precipitated, the increase in radius due to the remaining half of the solute is relatively small. The disadvantages of applying the fixed-radius solution are twofold:

First, fitting this equation to experimental data points yields only the product nr_0. This is a poor metric for comparing precipitation processes, since nr_0 can itself be a function of the initial impurity concentration and the impurity density in the precipitate.

Second, early in the precipitation process the precipitate radius may be increasing, giving rise to a nonexponential curvature. Specifying only the product nr_0 gives no information as to the nature of the first half of the precipitation process.

To obtain n and r_0 separately, some studies have used the conservation of mass to obtain n as follows. The conservation of mass is simply expressed as

$$\Delta c = \tfrac{4}{3}\pi r_0^3 n c_p \tag{7}$$

Combining Eqs. (5) and (7), one obtains an expression for n as

$$n = \left(\tfrac{3}{4}\pi \cdot \frac{1}{(4\pi D\tau)^3} \cdot \frac{c_p}{\Delta c}\right)^{1/2} \tag{8}$$

where Δc is the drop in solute concentration, and c_p is the density of the impurity in the precipitate. This approach is quite suitable for any process where the radius is fixed, as might be the case if iron precipitated on oxygen precipitates. Iterative techniques can provide much more flexibility and can model situations where n, r_0, and D are not necessarily constant. This will be discussed further in the section on computer modeling of gettering.

Given a density of precipitation sites, one can predict the precipitation rate using Ham's equations. However, before an impurity can precipitate, it must first form a stable nucleus. Transition metals nucleate heterogeneously on defects. Which defects are favorable heterogeneous nucleation sites will be discussed in the next section.

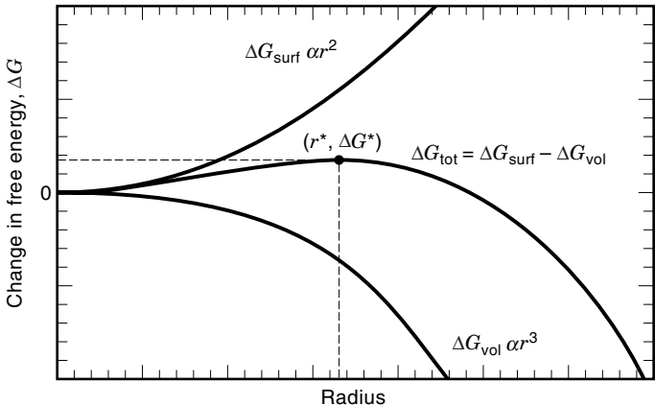

Figure 3. Schematic illustration of the competing energy terms involved in nucleation. Initially the surface term dominates for small radii, but at larger radii the volume term will dominate and precipitate growth is favorable. Thus, there exists a barrier to nucleation, ΔG^*. Defects can reduce this barrier by reducing the surface and/or strain energy, making nucleation at defects more preferred than in the bulk material.

Thermodynamics of Relaxation Gettering. From classical nucleation theory, there are two opposing forces in the nucleation process. The volume term, ΔG_{vol}, which promotes nucleation for supersaturated solutions, is proportional to the cube of the precipitate radius, r, and represents the energy gained when a given volume of precipitate is formed. Of course, the solute must be supersaturated; otherwise energy must be supplied to form the precipitate. The opposing term, ΔG_{surf}, is the energy required to form the interface between the precipitate and the host matrix, and thus is proportional to on the square of r and to the surface energy. Finally, for a misfitting precipitate, the misfit strain energy must also be included, and is also proportional to the cube of the precipitate radius, ΔG_{strain}. The misfit strain energy can oppose or enhance the nucleation of a precipitate, depending upon the strain state of the host matrix. If there is no strain in the matrix, then the creation of strain will oppose the formation of a nucleus. This can be expressed as

$$\begin{aligned} \Delta G &= \Delta G_{surf} - \Delta G_{vol} + \Delta G_{strain} \\ \Delta G &= \sigma\, 4\pi r^2 - \tfrac{4}{3}\pi r^3(\Delta G_v - \Delta G_s) \end{aligned} \tag{9}$$

where σ is the surface energy per unit area, ΔG_v is the energy gained in precipitating a unit volume of solute, and ΔG_s is the strain energy created per unit volume by the formation of the misfitting precipitate. A defect of any sort can act as a catalyst for nucleation by lowering the surface energy term and/or modifying the strain in the matrix. The energies are illustrated in Fig. 3. Initially the surface term dominates for small radii, creating a barrier to nucleation. The height of this barrier is denoted as ΔG^* and occurs for a critical radius r^*. At larger radii the volume term will dominate, making continued growth of the nucleus energetically favorable. For successful nucleation, a nucleus must therefore overcome the barrier to nucleation. Defects can help to lower this barrier by reducing the surface energy term or the strain energy term. Coulombic interactions between the precipitate and the dissolved impurity also have an effect on the nucleation and precipitation of metals. However, there exists no expression for the charge of the precipitate as a function of size.

Transition metals precipitate heterogeneously at structural defects such as oxygen precipitates, dislocations, stacking faults, and surfaces. To be clear in describing relaxation gettering processes, one should note that an oxygen precipitate or a dislocation is not in itself a gettering site. These defects can only act as heterogeneous nucleation sites for a silicide precipitate. The silicide precipitate, once formed, is then the gettering site. Thus there need not be a one-to-one correlation of defects and gettering sites, since nucleation depends upon supersaturation and on the barrier to nucleation of each defect present.

While the mechanism of internal relaxation gettering had long been thought to be precipitation at either dislocations or oxygen precipitates themselves, it began to be clear in the late 1980s and early 1990s that each metal has different precipitation behavior and precipitates preferably at different defects (69,70). Graff et al. (71,72) and Falster and Bergholtz (73) in 1990 compared the silicon surface as a heterogeneous precipitation site with oxygen-related defects in the bulk for Cu, Ni, Pd, and Co. For some metals and conditions, the oxygen-related defects were more favorable precipitation sites and prevented haze formation, that is, precipitation at the surface (74). In addition to earlier studies on copper precipitation at dislocations, Gilles et al. (75) in 1990 indicated that iron precipitated at oxygen precipitates, Falster et al. (76) in 1992 observed the different heterogeneous precipitation behaviors of Cu, Pd, and Ni in silicon, and Shen et al. (77) in 1994 showed that punched-out dislocations were more favorable precipitation sites than Frank partials for Cu and Ni. Qualitatively at least, one can thus begin to rank some structural defects by their barriers to nucleation, as is shown in Fig. 4 based upon work by Shen (77–80) and Falster (73,76). The diffusivity of the metal also plays an important role in

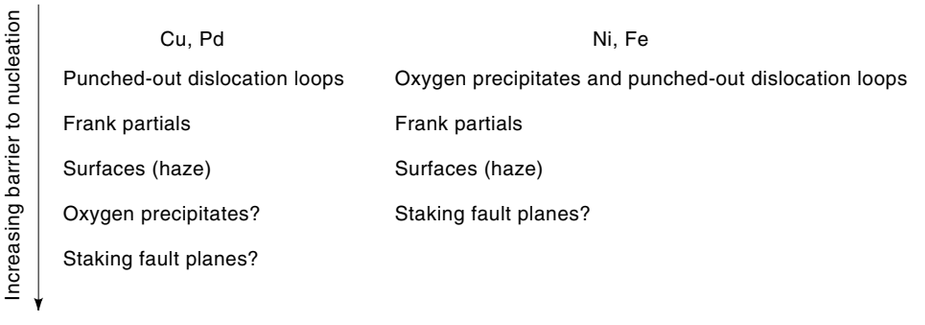

Figure 4. Qualitative ranking of heterogeneous nucleation sites based on Shen (77–80) and Falster (73,76). Defects near the top are more favorable nucleation sites. During a slow cooldown, metal impurities are expected to nucleate only at the top sites.

which defect sites are nucleated. A fast diffusing metal such as copper can move large distances to find the most favorable heterogeneous nucleation sites while slower metals such as iron may nucleate only at the nearest defect.

There is considerable uncertainty as to where grain boundaries would rank. A study by Ihlal et al. (53) correlated the energy of interfaces in bicrystals with gettering efficiency. This would indicate that high-energy boundaries are more favorable nucleation sites than low-energy boundaries. This is also in qualitative agreement with Shen's observation of copper nucleating preferentially at higher energy dislocations (punched-out dislocations) than on lower-energy dislocations (Frank partials).

Additionally, the cooling rate has a significant influence on the type and number of precipitation sites. A slow cooling rate results in a small supersaturation, and thus a small driving force for precipitation. In this case, nucleation is expected to occur on only the most favorable sites. Fast cooling rates create high supersaturations, and nucleation could occur at any and all structural defects present. Studies by Shen et al. (77–79) on Cu, Fe, and Ni, using slow and fast cooling rates, have illustrated exactly this type of behavior (78,81–83). Hieslmair et al. (84,85) predicted optimal linear cooling rates on the basis of experimental data on iron precipitation and computer simulations.

Possible Segregation to Structural Defects. As described above, a defect can lower the barrier to nucleation. Often in the literature, the gettering mechanism itself is not specified and impurities are simply assumed to be trapped at defects. Terms such as "trapping" and "decoration" imply that an impurity need not be precipitated in order to be fixed at a structural defect. Such terminology implies that metal impurities segregate to structural defects. Whether or not this is the case is difficult to ascertain experimentally, but possible mechanisms for such behavior are as follows:

- Many structural defects (grain boundaries, dislocations) have dangling bonds, which could bind impurities. Since most silicon bonds in structural defects are reconstructed, the dangling bond density is low, limiting the total amount of impurity that can be gettered in this manner. Additionally, it would be difficult to detect such decoration.
- Electron orbital interactions between interstitial impurities and the surrounding silicon atoms partly determine the solubility of an impurity. It is clear that by altering the structure of the silicon matrix, the electron orbital interactions are affected (61) and can change the solubility of an interstitial impurity as discussed above in the section on solubility. Baldi et al. (86) viewed the disorder caused by structural defects as approximating the liquid silicon structure and thus expected some amount of segregation, as is observed between solid and liquid silicon.
- The nature of the charge state of dislocations can have an effect on ionized metal impurities. This coulombic trapping would depend on the Fermi level and the specific impurity. Neutral impurities would thus not segregate to dislocations.
- Segregation of metal impurities to structural defects due to interaction of the metal and the strain has also been suggested (87). However, assuming the strain energy of a dislocation is the interaction energy, Sumino (88) showed that this interaction energy cannot significantly bind impurities at room temperature.
- Cahn (89) derived expressions for the activation energy of nucleation on a dislocation. He showed that the dislocation strain-energy term is favorable for nucleation only for small precipitate radii, while the volume term is favorable for nucleation for large radii. If there is not sufficient overlap between the two terms, it is in principle possible that very small nuclei are stable yet will not grow without a large supersaturation.

All of the segregation processes outlined above have a limited capacity for metals, and probably become saturated during any intentional metal contamination step common to gettering studies. Therefore, segregation effects appear to be minor in comparison with the relaxation (precipitation) processes during gettering. "Copper decoration" is a commonly used term in many studies. However, it is copper precipitation on defects that is actually observed in many studies. Considering the extremely fast diffusion coefficient of copper (90), it would be easy to mistake a segregation/trapping effect for what is actually precipitation even with a fast cool down.

The recombination activity of dislocations appear to be extremely sensitive to metal contamination. Numerous studies have attempted to understand the interaction of low levels of metal impurities and dislocations by using electron-beam-induced current (EBIC) (83,88,91–93). It is difficult to draw definite conclusions about segregation of metals to structural defects, but it seems reasonable to state that there appears to be a segregation of small amounts of metal impurities to structural defects. Still, these and other studies have established that dislocations do act as heterogeneous nucleation sites and precipitation is a significant gettering mechanism.

Strain and Relaxation Gettering. The role of strain produced by structural defects in enhancing the precipitation of metals has been discussed (94,95). Strain around a defect enhances or inhibits the formation of a silicide depending on whether the silicide precipitate can relieve or exacerbate the strain as in the following reaction:

$$M_{int} \rightleftharpoons M_{precip} + \{strain\} \tag{10}$$

For example, a compressive strain around an oxygen precipitate would enhance the formation of a silicide with a greater silicon density than the silicon matrix itself. Thus, it would be energetically favorable for $FeSi_2$ to precipitate around oxygen precipitates, since this silicide has a smaller molar volume and will relieve some of the strain. On the other hand, Cu_3Si would not be expected to precipitate at oxide precipitates since this would increase the total strain in the silicon matrix. McHugo et al. (54) indicated that strain around the oxygen precipitate could enhance iron precipitation and inhibit re-dissolution of gettered iron, thereby stabilizing the gettered iron. Furthermore, not all precipitates have exactly the same amount of strain around them, and the strain is not even uniform around a single oxygen precipitate. It should also be pointed out that the enhancement or inhibition of precipitation of silicides due to strain does *not* indicate that the solubility of the metal has changed. The solubility is always

defined with respect to an *unstressed* surface silicide. Strain-enhanced or inhibited precipitates represent a different boundary condition and will result in different equilibrium concentrations of dissolved impurities. The effects of strain on solubility include electron orbital interactions and have been discussed in the section on solubility.

A quantitative analysis of heterogeneous nucleation sites is difficult. Work done to date allows for qualitative comparisons between a few types of defects at best. Optimally, one would like to be able to obtain some kind of distribution of barriers to nucleation for a given type of defect. In order to obtain such a distribution, however, many factors must be taken into account (supersaturation, strain, nucleation site and precipitate geometries, electronic effects, etc.).

Internal Gettering

Because of its relevance to internal gettering and creation of detrimental surface defects, oxygen nucleation and precipitation in silicon have been studied for many years (a comprehensive treatment is given by Ref. 96). The objective of most internal gettering techniques was to create a denuded zone (DZ) near the surface or device region and then to nucleate and grow oxygen precipitates in the bulk of the wafer. The DZ is, in principle, a defect-free zone with no oxygen precipitates. The DZ can be formed by heating the wafer to high temperatures to allow the dissolved oxygen to diffuse out of the wafer. After this outdiffusion, the resulting oxygen concentration in the surface region is significantly lower than the bulk concentration. Thus, during a subsequent lower-temperature anneal, nucleation of oxygen only takes place in the bulk (64). The last step is to grow the oxygen precipitates at a high temperature. Following these guidelines, many time–temperature recipes have been proposed, (97–103) but repeatability and uniformity have always been difficult to achieve. There were differences in the oxygen precipitation behavior within a wafer, between wafers from different sections of a Cz ingot, and between different wafer vendors (104). Thus the history of the wafer, including the time–temperature history during ingot cooling, influenced oxygen precipitation. Typically, the time–temperature treatment of a wafer for internal relaxation gettering is as follows:

- Annealing above 1050°C for the outdiffusion of oxygen and formation of DZ
- Annealing below 800°C for between 3 h and 24 h to nucleate oxygen precipitates
- Annealing above 950°C for between 1 h and 16 h to grow the oxygen precipitates

Ramped temperature treatments were also used (105) to further accelerate the oxygen precipitation process.

Recently, however, Falster et al. (106) have developed a method to reliably and uniformly control and nucleate oxygen in silicon wafers by controlling the excess vacancy concentrations. The first step is to anneal the wafers at high temperatures (1200°C for 10 s) to erase the thermal history of the wafer. At this temperature, there exists an equilibrium concentration of vacancies and silicon interstitials such that the vacancy concentration exceeds the interstitial concentrations. By carefully controlling the annealing temperature, the cooling rate, and the ambient gas, the final vacancy profile can be manipulated so that there remains an excess concentration in the bulk and very low concentrations near the surfaces. The general shape of the vacancy concentration is followed by the oxygen precipitation behavior. Apparently, not only is outdiffusion of oxygen not required for DZ formation, but the oxygen precipitation behavior is completely decoupled from the oxygen concentration itself and is controlled by the vacancy concentration. When the vacancy concentration comes to dominate the oxygen clustering behavior, the normally very strong oxygen concentration dependence of precipitation disappears.

Thus, a structure with a DZ on the surface and oxygen precipitates in the bulk can be formed reliably. The oxygen precipitates also produce other structural defects such as punched-out dislocations and stacking faults depending on the precipitate growth conditions. A compressive strain field will also surround oxygen precipitates, since the density of silicon in the SiO_2 precipitate is approximately half that in the silicon matrix. Which sites are the most favorable precipitation sites depends upon the metal impurity, the cooling rate, and the silicide precipitate density. Generally, all metals were observed to precipitate on almost any defects when quenched from high temperatures. Under such conditions, however, the metals are certainly in metastable states, and often their crystal structures are ambiguous. Using slower cooling rates, particularly when the cooling rate is adjusted for the metal diffusivity, certain trends are observed. Clearly, high-silicon-density silicides can help relieve compressive strains and would thus be favorable in regions with high compressive strain fields such as near an oxygen precipitate. Low-silicon-density silicides require the emission of silicon interstitials, and nucleation of such a precipitate would be inhibited near an oxygen precipitate. Vanhellemont and Claeys (94) and Seibt (107) described this process for various metals and tabulated the required emission or absorption of silicon self-interstitials for the growth of metal precipitates. Based on these results and on results from Falster et al. (76), the precipitation behavior of metals can be approximately divided into two groups,

high-silicon-density silicides, which are either smaller or only slightly larger (within 2%) than the silicon matrix, and

low-silicon-density silicides, which are significantly larger than the silicon matrix.

Table 1 shows the expected composition and density ratio of several common metal impurities (94,107–110). The density

Table 1. Composition and Properties of Various Metals Silicides Expected to Form During Precipitation[a]

Metal	Expected Silicide	Density Ratio	References
Iron	$FeSi_2$	0.94	94,107
Nickel	$NiSi_2$	0.96	94,108
Cobalt	$CoSi_2$	1.0	108,109
Palladium	Pd_2Si	2.1	109
Copper	Cu_3Si	2.3	107–109

[a]The density ratio is the silicon density in the silicide divided by the silicon density in the bulk, 5×10^{22} Si/cm^3. A number less than 1 indicates the absorption of silicon self-interstitials during growth, while a number greater than 1 indicates emission of silicon self-interstitials during growth.

ratio is the silicon density in the silicide divided by the silicon density in the bulk, 5×10^{22} Si/cm^3.

High-Silicon-Density Silicides: Iron, Nickel, and Cobalt. Gilles et al. (75,111) in 1990 measured the low-temperature precipitation rate of iron and inferred nr_0, where n is the density of precipitation sites with a radius of r_0. They showed a direct correlation between the product nr_0 for oxygen precipitates during the oxygen precipitate growth step and that for iron in the same samples at low temperatures. This clearly established a link between iron precipitation and the presence of oxygen precipitates and indicated that iron was precipitating on the oxygen precipitate itself. TEM studies, however, failed to detect iron precipitates at the oxygen precipitate. In TEM studies on nickel precipitation, Falster et al. (76) and Bhatti et al. (112) observed that nickel precipitated at the silicon–oxygen precipitate interface on some of the oxygen precipitates. This precipitation enhanced the generation of punched-out dislocations, which then also served as nucleation sites. It is not clear how nickel precipitation enhanced the generation of punched-out dislocations. It would be expected that nickel precipitation would not add to the strain around the oxygen precipitate and could even help to relieve it. Shen et al. (37) observed that the presence of iron serves to enhance the nucleation of oxygen precipitates, suggesting iron can relieve some of the strain produced by the oxygen precipitate. Direct studies by Shen et al. (78) also showed the behavior of iron precipitation on stacking faults. McHugo et al. (54) showed that iron precipitates more slowly and is more easily re-dissolved from oxygen precipitates with no strain than oxygen precipitates with strain, indicating that the strain of the oxygen precipitate enhances gettering of iron. Hieslmair et al. (85) expanded on Gilles's work and showed that the iron precipitate site density matched the oxygen precipitate site density for over four orders of magnitude of oxygen precipitate density. The overall model of how iron precipitates is as follows.

- Given a slow enough cooling rate, oxygen precipitates are the primary nucleation sites. Punched-out dislocations are also expected to be favorable nucleation sites.
- No punched-out dislocations are expected to result from iron precipitation at oxygen precipitates.
- At higher cooling rates, iron precipitates at any nearby defects, including stacking fault planes.

Other faster diffusing metals in the high-silicon-density group precipitate at:

- Oxygen precipitates and punched-out dislocations which are the primary nucleation sites.
- Precipitation at the oxide–silicon interface adds stress and helps punch out dislocation loops, which glide far from the oxygen precipitate.
- These punched-out dislocation loops then serve as additional nucleation sites.

Recent experimental results of iron precipitation and computer simulations of gettering by Hieslmair et al. (85) predict that for a 4 μm DZ or epitaxial layer and a high concentration of oxygen precipitates, iron levels can be kept below 2×10^8 cm^3 with a cooling rate of about 70°C/min to a final temperature of 200°C.

Low Density Silicides: Copper and Palladium. Copper precipitation in silicon has been studied for over 40 years, beginning with studies by Dash (113) in 1956. Nes (114,115) and Solberg (116) described the manner in which copper repeatedly precipitated on dislocations. Tan et al. (64) in 1977 observed copper precipitation on punched-out dislocations from oxygen precipitates and proposed the idea of internal gettering. Seibt studied the precipitation of Cu on stacking faults (117) and proposed (95) that for effective gettering of copper, the silicon self-interstitial concentration must be taken into account. Falster and Bergholz (73) studied the gettering of copper and other metals by oxygen-related defects, observing the suppression of haze formed by surface precipitation of copper. Additionally Falster et al. (76) and Bhatti et al. (112) showed that Pd precipitation behavior is similar to that of Cu. Studies (15,76) also revealed that metals can be redissolved after they were precipitated (gettered) and can be gettered again. Shen et al. (77,78) have extensively investigated copper precipitation on various types of structural defects using different cooling rates. It was not until recently, however, that the intrinsic diffusivity of copper was determined (90) and could explain the very rapid precipitation of copper when cooling from high temperatures. With a migration enthalpy of only 0.18 eV, it is easy to see that copper atoms can diffuse large distances to favorable heterogeneous nucleation/precipitation sites even at room temperature.

These and other studies present a fairly cohesive model of copper precipitation and thus of internal gettering of copper. Essentially, copper

- precipitates in banded colonies in the absence of large oxide precipitates and/or dislocations and stacking faults. While punched out dislocations are preferred heterogeneous precipitation sites, copper will precipitate on Frank partials if the cooling rate is fast and punched-out dislocations are sparse.
- Dislocations are more likely to form around oxygen precipitates if Cu is present. Once formed, dislocations are good heterogeneous nucleation sites for copper precipitation.
- As copper nucleates and grows on dislocations, they kick out silicon self-interstitials which are absorbed at dislocations and force some segments to climb. These segments serve as fresh nucleation sites.
- The stress from the growth of copper precipitates causes dislocations to glide and intersect other dislocations, creating jogs. The final result of copper nucleation and growth and of dislocation nucleation, climb, and glide, is a dislocation tangle around the oxygen precipitate, on which further copper nucleation takes place. Thus, relaxation gettering for copper is enhanced when oxygen precipitates are grown in such a manner that punched-out dislocations are formed.

Since gettering depends upon a difference in precipitate site density, the copper precipitate site density should be studied as a function of oxygen precipitates and related defects. Laczik et al. (82), using scanning infrared microscopy

(SIRM), observed that the number of copper precipitates never exceeded 5×10^7 precipitates/cm^3 for even fast cooling rates (≈100°C/s) and large oxygen precipitate densities (≈ 10^9 precipitates/cm^3). This was explained as a kind of instant Ostwald ripening effect. As the metal nucleates on a favorable site, the metal concentration in the vicinity of the site drops. This reduces the driving force for precipitation at other sites nearby, precluding nucleation on any sites within a diffusion length of the original site. Since copper and nickel are fast diffusers, the diffusion length is large. This model would predict that, given a high density of nucleation sites, the number of copper precipitates is a direct function of the cooling rate. This type of model may also explain the temperature dependence of the iron precipitation site density observed by Hieslmair et al. (84).

So far, metal precipitation has been studied individually. Coprecipitation of metals is certainly possible and in some cases is expected to be favorable. Seibt (95) observed copper and iron coprecipitation. To the best of the author's knowledge, no study has focused on coprecipitation of metals. This is certainly a weakness of gettering studies, since there is usually more than one metal contaminant in practical applications. Additionally, there has been speculation that iron is reacting with oxygen precipitates and forming a silicate rather than precipitating on oxygen precipitates and forming a silicide (118–120).

Back-side Polysilicon and Damage Gettering

Surface damage gettering was demonstrated and discussed by Mets (63) as early as 1965. He used surface damage from sandblasting to repress bulk precipitation of copper and improve *pn*-junction leakage currents. He likened the damage region to a sponge for impurities such as copper. Studies and observations of copper precipitation on dislocations (64,114,116) in the 1970s did not affect the concept of damage regions acting as a sponge. Baldi et al. (86) likened the disorder in structural defects to a more liquidlike structure and expected a segregation effect similar to that between solid and liquid silicon. As a consequence, most of the studies on back-surface gettering assume segregation-type (sponge) behavior and, more often than not, overlook the possible relaxation (precipitation) aspects of back-side gettering. Many studies continue to this day in this tradition (66,67,86,121–124) and often neglect to mention the cooling rate used in the study. Thus, there are currently three models for back-side gettering:

- Back-side treatments provide an abundance of heterogeneous nucleation sites for precipitation of metal impurities (39,125–127).
- Back-side gettering is a segregation-based technique such that metals become trapped at the defects at high temperatures and/or without supersaturation [Refs. 66,121–124,128; for a discussion of segregation to dislocations, see Sumino (129)].
- Back-side treatments enhance the precipitation of oxygen precipitates by absorbing silicon self-interstitials (130). Back-side treatments essentially enhance internal gettering (131). This idea fits well with other studies that observe that oxygen precipitation is sensitive to the silicon self-interstitial concentration (132).

Earlier discussions in this work have given a basis for segregation of metals to grain boundaries and dislocations. The difficulty is that these particular segregation mechanisms have a finite capacity for capturing impurity metals, which become saturated when one intentionally contaminates silicon samples at high temperatures, as is often done in gettering studies. Therefore, the segregation gettering mechanism may play a role when low levels of contamination are present, as might be the case when actual device yields are correlated with back-side treatments (86,121). Some studies, however, intentionally contaminate silicon samples and attempt to report on segregation effects.

Precipitation of metals in the back-surface gettering layer is expected to proceed as described in the previous section. Cooling rates are very important, since the metals must diffuse through the wafer to precipitate at the back surface. While this is not problematic for copper or nickel, back-side gettering of iron may not be feasible because of the very slow cooling required (133). Sadamitsu et al. (118) and Ogushi et al. (124) have performed isothermal studies on gettering of iron by poly back seal (PBS) and have shown long annealing times of the order of 30 hours at 600°C to reduce initial iron levels from 1.5×10^{12} to 3×10^{10} Fe/cm^3.

Back-side damage gettering may no longer be a viable gettering technique, since the damage introduces particulate contaminants further into the process line. To reduce particulate contamination levels, 300 mm wafers may have a polished back surface to reduce particulate generation, entrapment, and shedding (134). Thus polysilicon layer gettering may be the only viable back-side gettering technique in the future.

SEGREGATION GETTERING

General Mechanism

Considering gettering as a three-step process of release from the original site, diffusion, and capture into the gettering layer, the critical step for segregation gettering is the capture process. The release process has only recently been studied but the initial results indicate release can be rapid with no observable barrier (26). Furthermore, while the diffusion of the impurities to the gettering layer is often the rate-limiting step for gettering (27), the capture process in segregation gettering defines how many impurities can be gettered, i.e., how effective the gettering can be. The ability of a gettering region to segregate impurities is quantified by a segregation coefficient, S, given by

$$S = \frac{C_g}{C_d} \tag{11}$$

where C_g and C_d are the impurity concentrations in the gettering and device regions, respectively, under thermodynamic equilibrium conditions. The relative thicknesses of the device and gettering regions affect the total amount of impurities that can be gettered. Assuming a constant amount of impurity remains in the wafer during a heat treatment, the final thermodynamically equilibrated concentration of the impurity in the device region, C_{fd}, can be given as

$$C_{fd} = C_{id} \frac{1}{1 + S t_g / t_d} \tag{12}$$

where C_{id} is the initial impurity concentration in the nongettering region, and t_g and t_d are the thicknesses of the gettering and device regions, respectively. From this equation we clearly see that a gettering region will not completely remove all impurities from the device region after a gettering heat treatment. Rather, only a fraction is removed, depending on the initial contamination level, the segregation coefficient, and the relative thicknesses of the device and the gettering region.

The ideal temperature for segregation gettering depends on the temperature dependence of the segregation coefficient and diffusion coefficient for the impurity (42) as well as the time duration of the gettering anneal (136) and the initial level of contamination. In general, as the gettering temperature is increased, the diffusion coefficient will increase (increase in kinetics of gettering), while the segregation coefficient will decrease due to the rapid increase in impurity solubility in the silicon substrate relative to the impurity solubility in the Al layer (decrease in thermodynamic driving force). Figure 5 is a schematic representation of the optimal gettering temperature, with time dependence. As longer gettering times are used, the optimal temperature will decrease until all impurities are gettered (maximum gettering efficiency). A number of researchers (29,42,136–139) have noted different optimal gettering temperatures for impurity removal in single-crystal and polycrystalline silicon. These variations are most likely due to differences in gettering times and impurity type.

Segregation gettering of impurities in a semiconductor can be accomplished by numerous methods. For silicon substrates, the most commonly used methods are gettering by heavily doped substrates and by phosphorus and aluminum, all of which are discussed in more detail below.

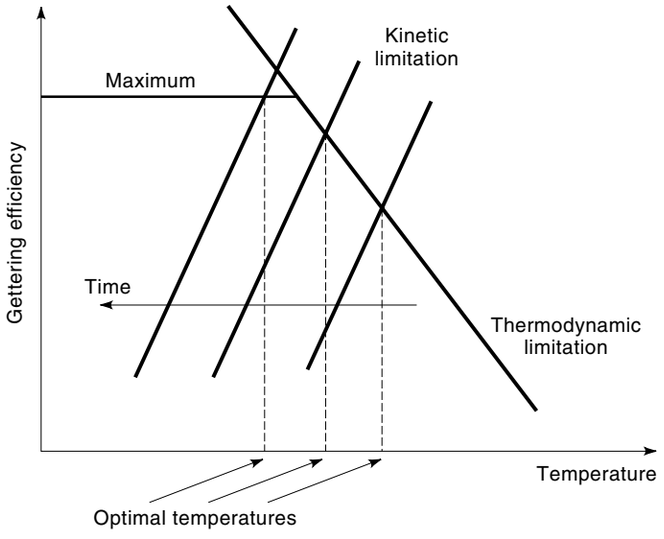

Figure 5. Time and temperature dependence for optimal gettering. High-temperature gettering is limited thermodynamically by the segregation coefficient, and low-temperature gettering is limited by the kinetics of impurity diffusion. Note that the optimal gettering temperature shifts to lower temperatures and the gettering efficiency increases with increased gettering time. Maximum gettering efficiency is reached when all impurities are removed.

Gettering by Heavily Doped Substrates

Effective gettering of metal impurities can be achieved with heavily doped substrates. Epitaxial layers ≈10 μm thick with low to moderate doping are deposited on the substrates in order to provide an active region for IC devices. The substrates are typically doped with boron, phosphorus, or arsenic, depending on the device application. The heavy doping increases the solubility of metal impurities such that segregation gettering results between the epi-layer and substrate. The heavy doping additionally acts as a sink for stray currents between IC devices, thus retarding latchup problems (104). Heavily-doped-substrate gettering belongs to a category of gettering techniques known as proximity gettering because the sink for impurities is located a short distance from the active device region. The close proximity of the gettering layer to the device region is advantageous because the thermal budget required to getter is minimal. Moreover, heavily doped substrates are significantly thicker than the device region, which makes a significant difference in the amount of impurities removed from the device region, as referred to above in Eq. (12). Gettering with heavily doped substrates holds an additional advantage over internal gettering in that internal gettering sites are widely dispersed over the area of the wafer, while heavily doped substrates create a continuous areal sink for impurities. This advantage manifests itself in shorter anneals for complete gettering to occur in heavily doped substrate gettering as compared to internal gettering.

Historical Aspects and Performance. Hall and Racette (55) were the first researchers to directly measure enhanced solubility of a metal impurity in heavily boron-doped silicon wafers. Specifically, they measure increased Cu concentrations with boron doping of 10^{18} at./cm^3 to 4.3×10^{20} at./cm^3. These enhancements increased with decreasing temperatures for the temperature range of 300°C to 700°C. Cagnina (141) and O'Shaughnessy (142) measured enhanced Au concentrations in heavily phosphorus- and arsenic-doped wafers for dopant concentrations greater than 10^{19} at./cm^3 in the temperature range of 1000°C to 1200°C. Later work has shown increased solubilities of Fe, Mn, and Co (40) and Fe in heavily doped silicon. Taken together, these results suggest heavily doped substrates can provide an excellent means of proximity gettering. In fact, studies of IC device performance by Gregor and Stinebaugh (143) and Cerofolini et al. (144) showed increased performance with the use of heavily exitaxially doped wafers. Since this early work, researchers have directly measured removal of impurities from epitaxial layers with the use of heavily boron-doped substrates (p/p^{++} wafers) (145–148). Additionally, Fe has been removed from lightly doped wafers with the use of heavily boron-doped back-side layers only 1 μm thick (149). However, p/p^{++} wafers were shown not to effectively remove Mo from the epitaxial layers (147).

Comparison with other Gettering Techniques. In comparison with other gettering techniques, heavily doped substrates are one of the most effective means to getter impurities. IC device characteristics have been shown to be better for p/p^{++} or n/n^{++} wafers than for internal gettering (143,144). Furthermore, Aoki et al. (146) demonstrated that p/p^{++} wafers were more effective in removing Fe from the device region than internal gettering for moderate to low contamination levels at

a 1000°C gettering temperature where the Fe was not supersaturated during the anneal. These results clearly show the advantages of segregation gettering over relaxation gettering.

Mechanism of Gettering: Heavily Doped Substrates

Fermi Level Effect. Gettering by heavily doped substrates operates by a number of mechanisms. The first is solubility enhancement via the Fermi level effect, driven by a solubility increase of positively or negatively charged impurities in the p^{++} or n^{++} substrates, respectively. The enhancement in charged species was proposed by Reiss et al. (45,46) as well as Shockley et al. (47,48). The essence of the Fermi level effect is that the solubility of charged metal impurities depends on the position of the Fermi level while the solubility of neutral impurities is independent of the Fermi level. Therefore, the total solubility of an impurity can be enhanced with a variation in the Fermi level. An example is Fe in boron-doped silicon, which has a donor state 0.39 eV above the valence band and therefore can become positively charged to a large extent when the Fermi level is below 0.39 eV. The solubility of the positively charged species is:

$$\frac{N_{\mathrm{Fe}^+}}{N_{\mathrm{Fe}_0}} = \frac{1}{2}\exp\left(\frac{E_\mathrm{D} - E_\mathrm{F}}{kT}\right) \tag{13}$$

where N_{Fe^+} is the concentration of positively charged Fe atoms, N_{Fe^0} is the concentration of neutral Fe atoms, $E_\mathrm{D} - E_\mathrm{F}$ is the position of the Fermi level with respect to the Fe donor energy level, and k is the Boltzmann constant. Heavy boron doping can significantly increase $E_\mathrm{D} - E_\mathrm{F}$ even at elevated temperatures, leading to an increase in the Fe^+ concentration and thus the total Fe concentration in the heavily boron-doped wafer.

It must be noted that donor level positions in the bandgap of semiconductors are typically measured at room temperature and not at elevated temperatures; therefore, the impurity enhancement by the Fermi level effect is typically estimated. By implementing the following charge neutrality and charge equilibrium relationships, one can then derive a useful relationship between the boron concentration and the positively charged impurity concentration:

$$N_{\mathrm{imp}+} = N_{\mathrm{imp}+,\mathrm{i}}\frac{N_\mathrm{A} + \sqrt{N_\mathrm{A}^2 + 4n_\mathrm{i}^2}}{2n_\mathrm{i}} \tag{14}$$

where $N_{\mathrm{imp}+}$ is the concentration of positively charged impurities in the heavily boron-doped silicon, $N_{\mathrm{imp}+,\mathrm{i}}$ is the concentration of positively charged impurities in intrinsic silicon, N_A is the concentration of negatively charged boron, and n_i is the intrinsic carrier concentration. The total impurity concentration N_tot will be

$$\begin{aligned} N_\mathrm{tot} &= N_{\mathrm{imp,i}} - N_{\mathrm{imp}+,\mathrm{i}} + N_\mathrm{imp} \\ &= N_{\mathrm{imp,i}} + N_{\mathrm{imp}+,\mathrm{i}}\frac{N_\mathrm{A} + \sqrt{N_\mathrm{A}^2 + 4n_\mathrm{i}^2} - 2n_\mathrm{i}}{2n_\mathrm{i}} \end{aligned} \tag{15}$$

where $N_{\mathrm{imp,i}}$ is the total impurity concentration in intrinsic material at the temperature of interest. Of particular note is that the solubility enhancement occurs as the ionized boron concentration N_A exceeds the intrinsic carrier concentration n_i. As N_A becomes much greater than n_i, the total impurity concentration is linearly proportional to the ionized boron concentration. As mentioned above, to obtain absolute concentrations, the position of the impurity donor level in the bandgap must be known at the gettering temperature.

Ion Pairing. Solubility enhancement via ion pairing occurs by coulombic attraction of the charged impurity atom to the charged dopant atom of opposite sign. Pairing occurs between metal impurities and dopants such as B, Al, and Ga and possibly with P and As dopants as well. An example of a pairing reaction between an impurity and a boron dopant is shown below:

$$\mathrm{Imp}_0 + \mathrm{h}^+ + \mathrm{B}^- \rightleftharpoons \mathrm{Imp\text{–}B} \tag{16}$$

where Imp_0 is the neutral impurity, h^+ is the hole that positively charges the impurity atom, B^- is the negatively charged boron atom, and Imp–B is the final impurity–boron pair. Clearly, ion pairing requires the creation of positively charged species, a result of the Fermi level effect. It must be noted that the pairing mechanism is not entirely a coulombic interaction, since the binding energies of Fe to B and to Al differ by approximately 0.15 eV (50,51). The importance of ion pairing and that of the Fermi level effect will be compared later.

From this reaction and the mass action law, an equation for the expected pair concentration is given by:

$$C_\mathrm{pair} = KN_D\mathrm{cc}N_{\mathrm{imp0}} \tag{17}$$

where C_pair is the concentration of impurity–boron pairs, K is the reaction constant, N_D is the concentration of charged dopant atoms, cc is the concentration of charge carriers (holes or electrons), and N_{imp0} is the concentration of neutral impurities. Invoking the charge neutrality and the charge equilibrium relationships from above, it follows that

$$C_\mathrm{pair} = KN_{\mathrm{imp}+,\mathrm{i}}(N_D^2 + N_D\sqrt{N_D^2 + 4n_\mathrm{i}^2})/2n_\mathrm{i} \tag{18}$$

where n_i is the intrinsic carrier concentration. If the charged dopant concentration is significantly larger than the intrinsic carrier concentration, then the concentration of impurity–dopant pairs scales as the square of the charged dopant concentration. This compares with a linear increase via the Fermi level effect.

The pairing of Fe with B has been studied and modeled (49,50,150). The pairing has been found to follow the relation below at or near room temperature:

$$[\mathrm{Fe_iB_s}] = [\mathrm{Fe_i^+}][\mathrm{B_s^-}] \times 10^{-23}\exp\left(\frac{0.65 \pm 0.02\,\mathrm{eV}}{kT}\right) \tag{19}$$

where $[\mathrm{Fe_iB_s}]$, $[\mathrm{Fe_i^+}]$ and $[\mathrm{B_s^-}]$ are the concentrations of Fe–B pairs, positively charged interstitial Fe, and negatively charged substitutional B, respectively, and k is the Boltzmann constant. One must note that this relationship may not be valid at elevated temperatures.

Fe–B pairing becomes statistically improbable at elevated temperatures (>200°C) but with very high boron doping levels ($>10^{19}$ cm^{-3}) the pairing can still affect the total impurity concentration. Considering only the Fermi level effect, one would expect the relation of Fe solubility to boron doping level as shown in Fig. 6. We see the strong temperature dependence of this enhancement effect as well as the strong depen-

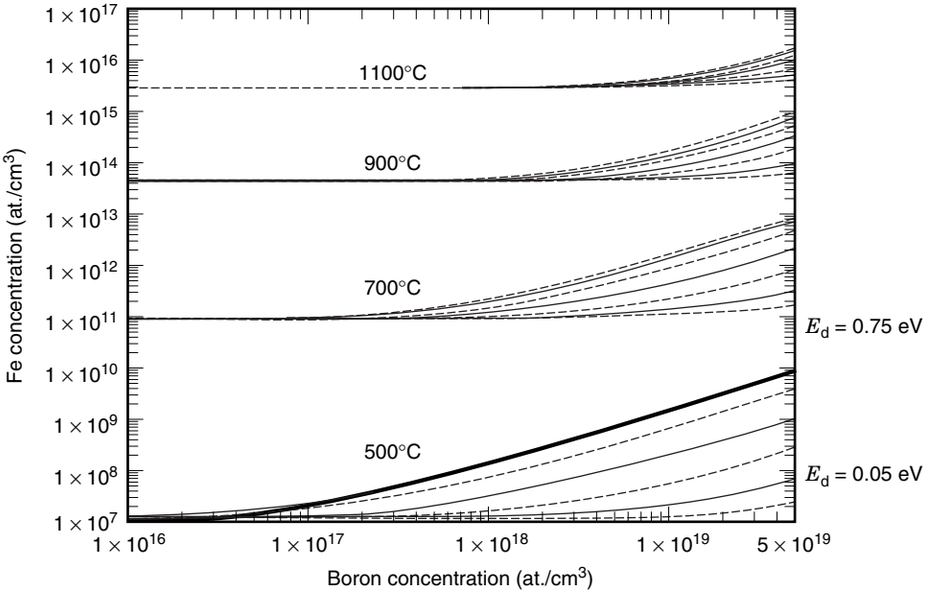

Figure 6. The theoretically expected Fe solubility in boron-doped silicon according to the Fermi level effect for 500°C, 700°C, 900°C, and 1100°C. The position of the Fe donor level in the bandgap has been varied from the valence band edge (E_d = 0.05 eV) to the upper half of the bandgap (E_d = 0.75) in increments of 0.1 eV.

dence on the Fe donor level in the bandgap, especially at moderate to low temperatures. The enhancement due to ion pairing may be observed by comparing Fig. 6 with Fig. 7, where we have included the ion pairing effect in Fig. 7. We have assumed the relation for Fe–B pair concentrations holds for elevated temperatures. We see the Fe–B pairing has increased the Fe solubility by approximately one order of magnitude for 500°C, especially for B concentrations $>10^{19}$ atoms/cm^3, while little or no effect is apparent at 700°C, 900°C, or 1100°C.

From Figs. 6 and 7, we see the importance of the impurity energy level in the bandgap. Generally, energy levels of impurities are measured at room temperature which may not be accurate at elevated temperatures. However, studies by Gilles, Schröter, and Bergholz (56) have shown the Fe donor energy level shifts toward the valence at temperatures >700°C, while at 700°C the level is as it is measured at room temperature (0.39 eV above the valence band). McHugo et al. (58) have shown the Fe donor level shifts away from 0.39 eV and toward the valence band edge for temperatures ≥800°C, where the donor level is at 0.4 eV, 0.24 eV, 0.23 eV and near the valence band edge at 800, 900, 1000, and 1100°C, respectively. Considering this data with Fig. 7, we see the impurity enhancement via the Fermi level effect and ion pairing is significant at high doping levels ($>10^{19}$ cm^{-3}) and moderate to low temperatures (<800°C).

Dislocation Formation. Another possible gettering mechanism in heavily doped substrates occurs via misfit dislocation formation, which provides a relaxation gettering site. The misfit dislocations form because of the significant difference in lattice constant between heavily doped wafers and the epitaxial layers. Dislocation formation has been observed to oc-

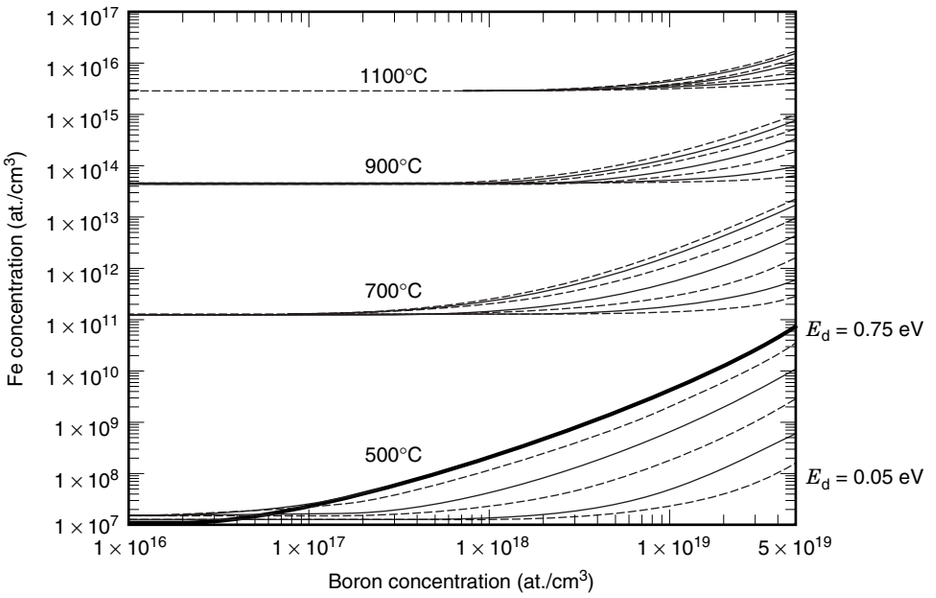

Figure 7. The theoretically expected Fe solubility in boron-doped silicon according to Fe–B pairing in conjunction with the Fermi level effect for 500°C, 700°C, 900°C, and 1100°C. The position of the Fe donor level in the bandgap has been varied from the valence band edge (E_d = 0.05 eV) to the upper half of the bandgap (E_d = 0.75) in increments of 0.1 eV.

cur for boron doping above 3×10^{19} at./cm^3 to 8×10^{19} at./cm^3 (151–153) and phosphorus doping above 5×10^{20} at./cm^3 (152,153). One must note that the thickness of the epitaxial layer also plays a role in the onset of dislocation formation (154).

Gettering of impurities to misfit dislocations has been observed (154). However, in general, the presence of misfit dislocations in the epitaxial layer is undesirable, since the dislocations may thread to the surface, thus causing deleterious effects in the device region.

Accelerated Oxygen Precipitation. An interesting phenomenon in heavily doped substrates is the acceleration of oxygen precipitation (155–157). This acceleration is expected to increase the oxygen precipitate concentration during a typical heat treatment, thereby increasing the amount of relaxation gettering in the bulk of the material (intrinsic gettering) as compared to a moderately to low boron doped substrate. However, while the high boron doping level may increase the oxygen precipitate density, it may leave the precipitates as inefficient gettering sites, as has been measured in highly carbon-doped silicon (54).

Boron–Silicon Precipitates. Of particular interest is the observation by Tomita et al. (149) of an extreme increase in gettered Fe into heavily boron-doped epilayers once the boron concentration became greater than the solid solubility of boron in silicon (10^{20} at./cm^3) even though no dislocations formed. In essence the electrically inactive boron created intense gettering. This work agrees with recent studies by Myers et al. (158) for high-dose boron implants. One may speculate that boron precipitates enhanced the gettering; however, further work on this subject should be pursued.

Phosphorus Gettering

Indiffusion of phosphorus into silicon has been shown to getter metal impurities such as Au (159–168), Fe (162,169), Cu (55,162,164,170), Co (171,172), Ni (169), and Pt (173,174). Phosphorus indiffusion gettering can be accomplished using the carrier gas $POCl_3$, other carrier gases such as PBr_3 (164) or P_2O_5 (169,170), or a spin-on source (42,170). A phosphosilicate glass (PSG) can form on the silicon surface when an oxidizing atmosphere is present. This glass acts as the doping source for the phosphorus indiffusion.

Historical Aspects and Performance. The first indirect observation of gettering by phosphorus indiffusion was by Goetzberger and Shockley (170), who found that soft diodes improved with deposition of either a phosphorus or a boron glass followed by heat treatment. Shortly thereafter, a direct measurement of the gettering effect was performed by Wilcox et al. (159,160), who found that high concentrations of phosphorus both hindered the diffusion of gold and increased its solubility. From this work, they suggested a vacancy interaction with the gold atoms, but compound formation of Au_2P_3 may also explain their measurements (159). In the same year Hall and Racette (55) measured an increased copper solubility in heavily phosphorus-doped wafers as well as heavily arsenic- and boron-doped wafers. They noted that phosphorus-doped wafers gave a greater solubility increase than arsenic-doped wafers, by a factor of 10 at 600°C and a factor of 3 to 4 at 700°C. From this observation they suggested some degree of ion pairing may be occurring in addition to the Fermi level effect, as suggested by Reiss (45) and Shockley and Moll (48). However, it must be noted that the arsenic-doped wafers did have a significant solubility enhancement, up to a factor of 1000. Thereafter, a number of researchers directly confirmed the phosphorus gettering effect (141,142,161,163,164,167,169, 171,172,175–178). Observations from these works are: (1) the impurity distribution follows the phosphorus indiffused profile (142,161,167); (2) dislocations form with extremely high phosphorus concentrations (153,161); (3) no metal impurity gettering occurs in the glass layer used for phosphorus indiffusions (164); (4) a relationship exists between the carrier gas used for glass formation (164), the growth speed of the glass layer (171), and the amount of impurities gettered; (5) precipitation of impurities in the phosphorus-doped layer (164,169); (6) SiP precipitates can form in the near surface region of the phosphorus-doped region (169,171,179) and (7) a high concentration of *substitutional* Co and Mn is observed in heavily phosphorus-doped regions (56).

Phosphorus gettering has been used to improve the performance of both single-crystal and polycrystalline silicon. Improvements in diode quality (162,170), I–V leakage (86,98,166), and minority carrier diffusion length (180,181) have been realized with phosphorus gettering of silicon used for integrated circuits. Additionally, great gains in solar cell performance have been achieved with phosphorus gettering (29,33,138,139,181–185). For polycrystalline solar cell materials, the response of the material to the phosphorus gettering treatment depends on the concentration of structural defects (29,138,184) as well as oxygen and carbon concentrations (29,139,182).

Comparison with Other Gettering Techniques. Phosphorus gettering is among the best gettering techniques. For instance, Cagnina (141) found that phosphorus-doped wafers had a higher solubility for metal impurities than arsenic or boron doped wafers, while Meek et al. (164) measured more impurities in phosphorus indiffused layers than in boron indiffused layers. In terms of material performance, phosphorus gettering has been seen to improve material better than back-side damage (86,98) and back-side polysilicon deposition (86). Additionally, phosphorus indiffusion gettering has been shown to improve diode characteristics as well as or better than internal gettering (98,143,144,186). Furthermore, phosphorus indiffusion getters more or approximately the same amount of impurities as implantation-induced gettering (163), and material properties are improved to a greater extent or approximately to the same extent as with implantation (143,144,186). Finally, the use of Cl (trichloroacetic acid) in the annealing gas during phosphorus in-diffusion slightly improves the material properties (143).

Cogettering. Some benefits are realized when phosphorus gettering is combined with another gettering technique. As will be discussed in more detail in the Al gettering section, a combination of phosphorus and aluminum gettering has been shown to greatly improve material performance beyond the use of one gettering technique (139,180,183,187,188). A synergistic gettering effect between phosphorus and aluminum gettering has been proposed (187) and some experimental results indicate this effect occurs (188). Finally, phosphorus gettering has been combined with Cl gettering. This is simply accomplished by adding trichloroacetic acid into the phosphorus annealing gas. Improvements have been realized for solar cells (184) and CMOS integrated circuit devices (143). The mecha-

nism for Cl gettering may be extraction of metal impurities from the surface/near-surface region of the silicon or removal of impurities from the annealing furnace.

Mechanism of Gettering: Phosphorus Gettering. A heavily doped layer of phosphorus provides a number of potential mechanisms for gettering: solubility enhancement by the Fermi level effect and ion pairing, gettering to dislocations, and silicon self-interstitial injection-assisted gettering. While the Fermi level effect and ion pairing certainly contribute to impurity solubility enhancements in phosphorus-doped silicon, these effects cannot fully explain the experimentally measured enhancements, suggesting other mechanisms are active. Details of each mechanism are discussed immediately below.

Fermi Level Effect and Ion Pairing. As discussed in the section on gettering by heavily doped substrates, solubility enhancement via the Fermi level effect is driven by a solubility increase of negatively charged impurities in the heavily phosphorus-doped region. The enhancement in negatively charged species was proposed by Reiss et al. (45,46) as well as Shockley et al. (47,48). Essentially, the total concentration of impurities is increased in heavily doped regions of silicon because the charged species concentration is increased while the equilibrium neutral species concentration is unchanged, equating to an increase in the total impurity concentration. An example is Au in phosphorus-doped silicon, which has an acceptor state 0.55 eV below the conduction band and therefore can become negatively charged with phosphorus doping. Using similar analysis of the Fermi level effect as demonstrated in the heavily doped substrate section, it can be shown that the solubility enhancement occurs as the ionized phosphorus concentration exceeds the intrinsic carrier concentration and, as the ionized phosphorus concentration becomes much greater than the intrinsic carrier concentration, the total impurity concentration is linearly proportional to the ionized phosphorus concentration. To obtain absolute concentrations, the position of the impurity acceptor level in the bandgap must be known at the gettering temperature.

Solubility enhancement via ion pairing occurs primarily by coulombic attraction of the negatively charged impurity with the positively charged phosphorus atom. Clearly, ion pairing requires the creation of negatively charged species, a result of the Fermi level effect, therefore ion pairing occurs only after the ionized phosphorus concentration becomes greater than the intrinsic carrier concentration, i.e., the impurities become negatively charged via the Fermi level effect.

Using ion pair analysis similar to that described in the heavily doped substrate section we see that as the positively charged phosphorus concentration becomes significantly larger than the intrinsic carrier concentration then the concentration of impurity–phosphorus pairs is proportional to the square of the ionized phosphorus concentration. This is in contrast to the impurity concentration increase via the Fermi level effect where the impurity concentration increase is linear with ionized phosphorus concentration.

The Fermi level effect and ion pairing are active during phosphorus gettering as shown by Cu and Au solubility studies on heavily doped phosphorus and arsenic wafers (55,141,142). Since the Fermi level effect and ion pairing are the only expected enhancement mechanisms in wafer studies (dislocation formation and self-interstitial injection are not active), these results show that the Fermi level effect and ion pairing do affect the impurity solubility. It is also interesting to note that these studies show arsenic-doped wafers enhance the impurity solubility but to a lesser extent than phosphorus-doped wafers, especially at lower temperatures, indicating pairing is more intense with phosphorus doping (55,141). The fact that arsenic doping does getter impurities is contrary to later works, which discount the Fermi level effect based on a comparison of material performance after arsenic and phosphorus indiffusion gettering (42,144,186). These works are a qualitative comparison with other factors, such as unintentional contamination, potentially confusing the analysis.

In order to assess the functionality of the Fermi level effect and ion pairing in completely explaining phosphorus gettering, we have compared experimentally measured impurity concentrations as a function of phosphorus concentrations to the expectations from the Fermi level effect and ion pairing. Au data was used due to the extensive research on phosphorus gettering of Au.

A compilation of phosphorus gettering data at 900°C from Sveinbjörnsson et al. (167), Meek et al. (164) and Zimmermann et al. (174) is shown in Fig. 8 along with the theoretically expected Au solubility according to the Fermi level effect. Additionally, a compilation of phosphorus gettering data at 1000°C from Cagnina (141), Joshi and Dash (161), Meek et al. (164), and O'Shaughnessy et al. (142) is shown in Fig. 9 along with the theoretically expected Fermi level effect. The calculations of the Fermi level effect were performed up to 2×10^{20} P atoms/cm^3 in order to avoid complications once the Fermi level approaches the conduction band. The position of the Au acceptor level in the band gap has been varied from the valence band edge ($E_c - E_a = 0.8$ for 900°C and 0.75 for 1000°C) to the conduction band edge ($E_c - E_a = 0.05$) for the theoretical calculations. We see the Fermi level effect corre-

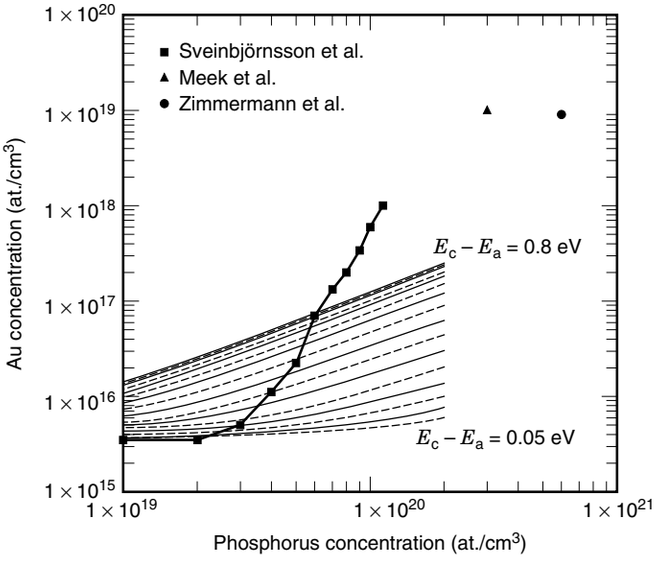

Figure 8. Phosphorus gettering data on Au at 900°C from Sveinbjörnsson et al. (167), Meek et al. (164), and Zimmermann et al. (174), along with the theoretically expected Au solubility according to the Fermi level effect. For the theoretical calculations, the position of the Au acceptor level in the bandgap has been varied from the valence band edge ($E_c - E_a = 0.8$) to the conduction band edge ($E_c - E_a = 0.05$) in increments of 0.05 eV.

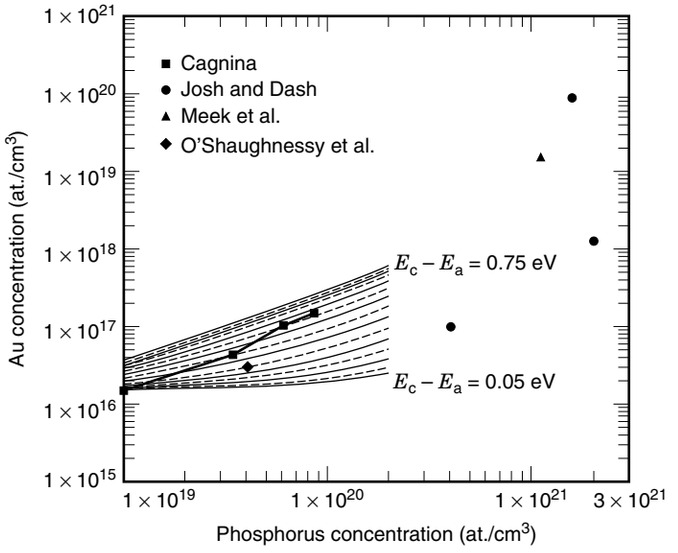

Figure 9. Phosphorus gettering data on Au at 1000°C from Cagnina (141), Joshi and Dash (161), Meek et al. (164), and O'Shaughnessy et al. (142), along with the theoretically expected Au solubility according to the Fermi level effect. For the theoretical calculations, the position of the Au acceptor level in the bandgap has been varied from the valence band edge ($E_c - E_a = 0.75$) to the conduction band edge ($E_c - E_a = 0.05$) in increments of 0.05 eV.

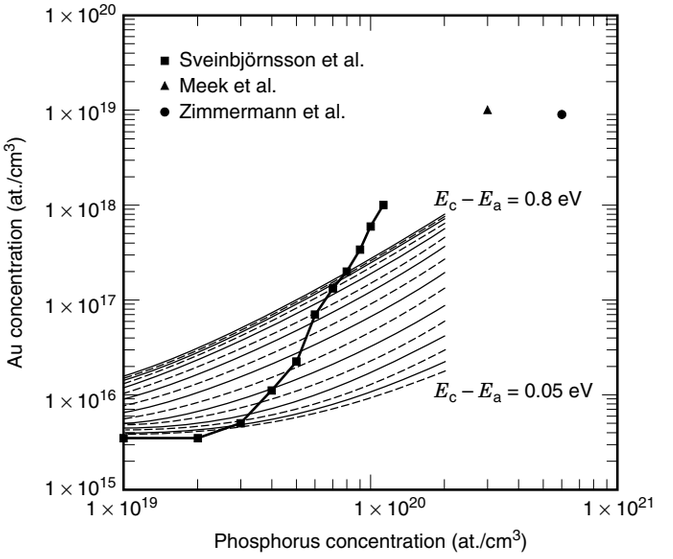

Figure 10. Phosphorus gettering data on Au at 900°C from Sveinbjörnsson et al. (167), Meek et al. (164), and Zimmermann et al. (174), along with the theoretically expected Au solubility according to the ion pairing effect in conjunction with the Fermi level effect. For the theoretical calculations, the position of the Au acceptor level in the bandgap has been varied from the valence band edge ($E_c - E_a = 0.8$) to the conduction band edge ($E_c - E_a = 0.05$) in increments of 0.05 eV.

lates fairly well with experimental data at 1000°C but poorly at 900°C.

Ion pairing, in conjunction with the Fermi level effect, may fully explain phosphorus gettering especially considering the ion-pairing effect scales as the square of the phosphorus concentration while the Fermi level effect has a linear dependence. Critical to calculating the Au concentration enhancement due to ion pairing is the reaction constant of the Au–phosphorus pairing reaction. Using the calculated reaction constant of Chou and Gibbons (10^{-20} cm^3) (176) we have calculated the expected Au enhancement in heavily phosphorus doped layers with the ion-pairing reaction and the Fermi level effect. Figures 10 and 11 are the results of these calculations. We see better agreement is achieved at both temperatures. The 1000°C calculations may completely explain all measured data, however, the 900°C calculations still cannot explain the measured data. Of additional note is the good agreement between theory and experimental data at low phosphorus concentrations only when the Au acceptor level is assumed to be fairly close to the conduction band, $E_c - E_a = 0.05$ eV to 0.3 eV. This may indicate a shift of the Au energy level toward the conduction band at elevated temperatures, which would agree in principle with the results of Gilles et al. (56) and McHugo et al. (58).

The discrepancy between experimental data and theoretical calculations may be explained when consideration is given to how the experimental data was taken. Specifically, the Au concentrations of Cagnina (141) and O'Shaughnessy et al. (142) were measured on phosphorus doped wafers while all other data was measured after phosphorus indiffusions. It seems the Fermi level effect and ion pairing can explain the amount of Au gettered into phosphorus doped wafers but cannot with indiffused phosphorus. This suggests phosphorus indiffusions produce an additional gettering effect, possibly via dislocation formation or self-interstitial injection or gettering at the phosphosilicate-silicon interface or SiP precipitates as has been suggested in the past (167,169,171,172, 177,178).

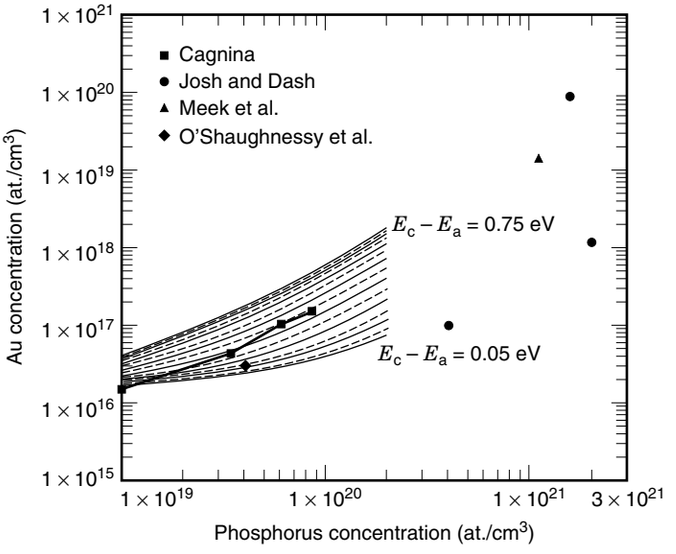

Figure 11. Phosphorus gettering data on Au at 1000°C from Cagnina (141), Joshi and Dash (161), Meek et al. (164), and O'Shaughnessy et al. (142), along with the theoretically expected Au solubility according to the ion pairing effect in conjunction with the Fermi level effect. For the theoretical calculations, the position of the Au acceptor level in the bandgap has been varied from the valence band edge ($E_c - E_a = 0.75$) to the conduction band edge ($E_c - E_a = 0.05$) in increments of 0.05 eV.

Dislocation Formation. Phosphorus has been observed to generate dislocations when indiffused to high concentrations in silicon (153,161,164,165,189). Yeh and Joshi have shown that phosphorus indiffusion induces a reduction in the silicon lattice constant by up to −1.8% (153). They attribute the lattice contraction to the smaller covalent radius of the phosphorus atom than that of the silicon in the lattice. In this same work, Yeh and Joshi observed dislocation formation as the phosphorus surface concentration exceeded 5×10^{20} P/cm^3. The dislocations were found to form a net of misfit dislocations located at a specific depth from the front surface. It must be noted that dislocation formation may depend on the total integrated dose of phosphorus in the indiffusion region rather than the surface concentration (189). Furthermore, the concentration limit of 5×10^{20} P/cm^3 should not be considered as a universal limit for dislocation formation. The phosphorus indiffusions of Yeh and Joshi were carried out with a solid phosphorus source in a nonoxidizing atmosphere, for which the strains may not be comparable to those induced by a gas source. Additionally, the indiffusions were only at one temperature, 1200°C, and so may not accurately represent dislocation formation at lower temperatures.

Numerous other studies have identified dislocation formation during phosphorus indiffusions. Joshi and Dash (161) and Meek et al. (164) have observed phosphorus-indiffusion-induced dislocation formation with the use of transmission electron microscopy (TEM). However, both research groups [Joshi and Dash with TEM, and Meek et al. with Rutherford Backscattering Spectroscopy (RBS)] observed precipitated gold only in the near-surface region, not in the dislocated region. Considering these studies, dislocation formation during phosphorus indiffusion does not seem to be significant in gettering Au impurities. However, Tseng et al. (165) measured an increase in the gettered Au concentration in the dislocated region of a phosphorus-*implanted* layer. However, the implant damage itself may account for the gettering action. In general, precipitation of impurities at dislocations would be expected to occur in the presence of an impurity supersaturation, which would occur during cooling, i.e., after the phosphorus indiffusion. Therefore, the amount of impurities gettered to the dislocations depends critically on the cooling rate after the phosphorus indiffusion.

Silicon Self-interstitial Injection. Phosphorus gettering may be assisted by silicon self-interstitial-injection. Phosphorus indiffusion has been observed to inject intrinsic point defects into the silicon bulk. Initially many researchers (86,156,164, 166,176,190,191) speculated that vacancies were injected during phosphorus indiffusion, creating enhanced diffusion of other dopants (emitter-push effect) (156,190,191). Additionally, point defect injection was thought to enhance the gettering action of the phosphorus layer by increasing the substitutional solubility concentration of metal impurities (86,164, 166,176). A review of this early work is given by Willoughby (192). Later, a number of phenomena were observed during phosphorus indiffusions that strongly suggested that phosphorus indiffusion injects silicon self-interstitials. Examples of the observed phenomena are extrinsic stacking-fault growth (193), dislocation climb (194,195), epitaxial regrowth of silicon at the phosphosilicate–silicon interface (169,179), oxygen precipitate dissolution (168) and vacancy defect (D-defect) dissolution (196). The mechanism may be the formation of SiP precipitates (169,171,179) that have an accompanying volume expansion or strain at the interface between the phosphosilicate glass (PSG)/silicon interface.

This self-interstitial injection has been used to explain the gettering effect of phosphorus indiffusion. Researchers (169, 171,172,177,178) provide a theoretical model and experimental results suggesting that self-interstitials play an important role in phosphorus gettering. Their model refers to the work of Gilles et al. (56), who observed a large increase of the Co substitutional species in the heavily phosphorus doped layer with indications of substitutional Co pairing with phosphorus. Furthermore, deep-level transient spectroscopy (DLTS) results from (56) suggested that the substitutional Mn species concentration greatly increased with phosphorus doping. From the results on Co and Mn, Gilles et al. inferred that the increase in Fe concentration in the heavily phosphorus-doped regions was also due to an increase in the concentration of substitutional Fe species. This increased substitutional concentration is possible if one supposes that the substitutional metal impurity has an acceptor energy level in the bandgap and therefore its concentration increases via the Fermi level effect discussed above.

With this increased substitutional species concentration in mind, the theoretical model (169,171,172,177,178), suggests phosphorus indiffusion produces a flux of self-interstitials into the silicon bulk *and* towards the PSG–silicon interface. The latter flux is due to the annihilation of self-interstitials at the interface, as may also occur for a bare silicon surface. The flux towards the bulk can enhance the diffusion of impurities (e.g. Au) and possibly increase the rate of precipitate dissolution. More crucial to the model are the self-interstitials near the PSG–silicon interface, which are speculated to *kick out* the substitutional metal impurities into an interstitial state. This is the same kickout mechanism related to impurity diffusion in silicon (197,198). The kickout of the impurity increases the interstitial species concentration of the metal impurity above the solubility limit, thus driving precipitation of the interstitial metal impurity either at the interface, as has been observed (169,179), or at another preferred precipitation site. Therefore, over time, the amount of precipitated metal impurity increases while the concentration of substitutional and interstitial metal impurities remains at a high level because of having a near-infinite source of impurities from the material bulk.

Analysis: Phosphorus Gettering Mechanism

The experimental observations of impurity gettering with phosphorus indiffusions (161,167,176) cannot be fully explained by the Fermi level effect and ion pairing. While the Fermi level effect and ion pairing are active they cannot fully explain the gettering phenomena from phosphorus indiffusions, as shown above in Figs. 8–11. Another mechanism is active but has not been clearly identified. Gettering of impurities to dislocations, formed by phosphorus indiffusion, can occur although the studies of Joshi and Dash (161) and Meek et al. (164) indicate little or no Au getters to these dislocations. Perhaps the best indicator of this unknown mechanism is from studies that show the phosphorus source/silicon interface plays an important role in phosphorus indiffusion gettering. Meek, Seidel and Cullis (164) observe slight differences in gettered Au concentrations when using either a $POCl_3$ or PBr_3 phosphorus diffusion source, implying the two

sources create a different interface condition. Furthermore, Kühnapfel and Schröter (171,172) show a factor of 7 increase in the amount of Co gettered when the phosphosilicate glass growth rate is increased above 3 nm/min. Additionally, they observe a factor of 7 increase in Co concentration at the silicon surface with simultaneous phosphorus doping and phosphosilicate glass growth (with no SiP precipitate formation) as opposed to only phosphorus doping, even though the surface concentration of phosphorus is the same for both boundary conditions. These results strongly suggest the silicon–phosphorus source interface plays an important role in phosphorus indiffusion gettering. Kühnapfel and Schröter suggest silicon self-interstitial injection is the cause for the gettering enhancement, with further embellishment of the model made later (178). However, further work should be performed with other impurities to confirm this concept.

Aluminum Gettering

Aluminum gettering occurs by deposition and subsequent heating of a thin Al or 2%Si–Al film on the back side of a silicon substrate. The Al layer getters impurities from the silicon substrate by segregation. Additionally, pitting or damage at the interface between Si and Al–Si may act as precipitation sites for metal impurities (33)—a form of relaxation gettering—although this mechanism has not been directly proven. Al diffusion into silicon also forms a p^+ layer, which can reflect electrons and avoid recombination at the back surface. This is generally known as the back-surface field (BSF) effect (199,200). Additionally, Al diffusion passivates grain boundaries (201) or dislocations to a great extent via rapid diffusion along grain boundaries (202). However, Martinuzzi et al. have obtained experimental results on Al gettering that indicate that material properties improve even without the benefit of pipe diffusion (203). Also, there is indirect evidence that Al accelerates production of atomic H, which is used for defect passivation (33,204).

Historical Aspects and Performance. The Al gettering phenomenon was first suggested by researchers who noted a marked increase in solar cell performance when annealing an Al layer on the back side of a silicon substrate (205,207). Orr and Arienzo (208) suggested gettering occurred even after relatively short anneals of 90 s. Thompson and Tu (209) were the first to directly observe Al gettering of metal impurities when they noted a significant accumulation of Cu in an Al layer on the back side of a silicon substrate following intentional contamination of the frontside of the substrate and subsequent heating. Since then, Al gettering has been shown to improve material properties in polycrystalline silicon used for solar cells in both thick substrates (28,29,33,137,201,210, 211) and thin film silicon (212) as well as in IC-grade single crystal silicon (29,32,135,203,213). Minority carrier diffusion lengths (L_n) in these materials can be increased by 100 μm to 200 μm, and overall solar cell efficiencies have been shown to increase by as much as 0.5% to 1%.

Comparison with Other Gettering Techniques. The efficiency at which Al gettering improves material quality has been compared with P gettering (183,188,214,215) as well as gettering to implantation-induced cavities (213). Al gettering performance is comparable to both P and cavity gettering. One advantage of Al gettering is its large capacity for impurities even with extended anneals. P gettering loses stability after long anneals via a decrease in the P peak concentration.

Cogettering. Material properties, such as L_n, have been shown to greatly improve for cogettering with P and Al (139,180,183,188,216). A synergistic effect has been measured experimentally (139,188) and explained theoretically (187). Mahfoud et al. (139) propose that the P layer getters Fe and Au while the Al layer getters Cu, thus providing the synergistic effect. Gafiteanu et al. (187) suggest the synergistic effect originates from the silicon self-interstitial injection by the phosphorus indiffusion, which accelerates the gettering process by increasing both the dissolution of metal precipitates and the diffusivity of some impurities. Furthermore, the gettering ability of the Al layer is significantly more stable than that of the P layer (due to continued P indiffusion and a decrease in the peak phosphorus concentration), so that when both mechanisms are combined the gettering action is enhanced.

Mechanism of Gettering: Aluminum Gettering. As mentioned above, aluminum gettering primarily operates by a segregation mechanism. Figure 12 is the phase diagram of the Al–Si system. The eutectic transition indicates that Al alloys with the silicon and will melt above 577°C. Below 577°C, the Al film will remain solid with the atomic percentage of silicon ranging from 0 to 1.59%. Both liquid and solid Al possess a solubility of 1 at.% to 10 at.% for many metals, including Fe, Cu, Ni, and Au, over a wide temperature range (217,218). This high solubility occurs even with a moderate concentration of silicon in the Al. Metal impurity solubilities in silicon are significantly lower and significantly decrease with decreasing temperature. For example, even at an elevated temperature of 1000°C, transition metal solubilities range from 0.000001 at.% to 0.001 at.% (1), therefore, a segregation coefficient of 10^3 to 10^9 is expected, depending on the metal impurity and temperature.

Direct measurements of the Al segregation coefficient have been made by Apel et al. (219) for Co in silicon and Hieslmair et al. (135) for Fe in silicon. Apel et al. found 10^3 as a lower bound for the segregation coefficient of Co between silicon and an Al layer at 820°C. Hieslmair et al. found segregation coefficients of 10^5 to 10^6 for Fe between silicon and an Al layer at temperatures from 750°C to 950°C. Each of these results is

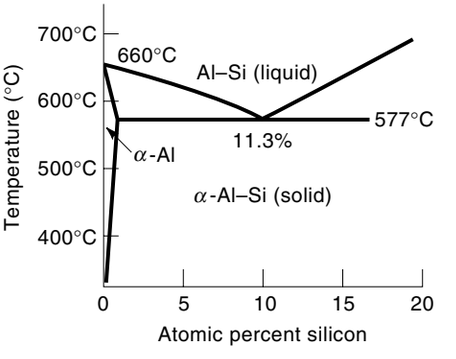

Figure 12. Phase diagram of aluminum and silicon. The α-Al phase is a solid solution of silicon in an aluminum matrix.

only a lower bound to the segregation coefficient, since in both experiments the gettering heat treatments were not sufficiently long to allow for complete diffusion of the impurities out of the substrate and into the gettering layer.

GETTERING BY IMPLANTATION

Metal impurities are gettered to implanted regions by either relaxation or segregation. Relaxation occurs either at implantation-induced damage or at clusters/precipitates of the implanted species. Segregation gettering results from the Fermi level effect or metal ion pairing with the implant species (e.g. phosphorus implantation), or at high concentrations of the implanted species, which essentially create a separate thermodynamic phase from the surrounding silicon, (e.g. a high boron implantation creating a boron–silicide precipitate) (158). This new phase can have a higher solubility for impurities than the silicon matrix, thereby driving segregation. A beneficial aspect of implantation gettering is the close proximity of the gettering layer to IC device regions, whereby gettering can occur with low thermal budgets. Additionally, the implant region provides a more uniform gettering layer than internal gettering, where the gettering sites are widely dispersed.

Gettering has been observed for implantation with silicon (163,165,220–222), phosphorus (163,165), carbon (223–229), oxygen (228), helium (228,230–236), hydrogen (222,237,238), boron (158,221,229,239), germanium (240,241), aluminum, and chromium (242). Typical implantation energies range from 50 keV to 10 MeV with implant doses ranging from 10^{13} at./cm^2 to 10^{17} at./cm^2. The implant damage (dislocations, stacking faults, point-defect clusters) for any implanted species will getter by a relaxation mechanism. However, gettering by segregation occurs as well, in particular for phosphorus, boron, helium, and hydrogen implantations. The phosphorus and boron implants create a layer of higher solubility than the silicon matrix, by means of the Fermi level effect and metal-impurity–dopant binding. Hydrogen and helium implantation form cavities centered at the projected range of the implant. During annealing at temperatures above 600 K, the gaseous species escape from the silicon matrix, leaving the cavities behind (243). The surfaces of the cavities are bare (unoxidized), allowing for segregation via chemisorption of metal impurities as well as precipitation. Metal impurities will chemisorb onto the interior surface before they will precipitate on the surface. The degree of chemisorption required before impurities precipitate depends on the binding energy of the impurity atom to the surface as compared to an impurity precipitate. It has been observed that the binding energy of copper and gold to the cavity surface is greater than to the precipitate (234,236), while the opposite is true for Fe and Co (232).

In general, implantation is an effective means to getter metal impurities. IC device characteristics have been shown to improve with various implantations (186,226,244). Compared to other gettering techniques, implantation getters a comparable amount of impurities. The true strength of implantation gettering is the close proximity of the gettering layer to the device region. This allows for rapid gettering of impurities away from the devices, as has been directly observed for boron- (239), carbon- (227), and helium-implantation-induced cavities (235). Comparisons of gettering capabilities amongst various implant species have been studied between Si- and H-implantation induced cavities (222,237), Si- and B- (221), Si-, B-, and C- (229), C-, O-, and He-implantation-induced cavities (228), as well as with Ar, O, P, Si, As, and B (163). The results of Wong-Leung et al. (222,237) indicate Au gettering to cavities is more effective than to silicon-implant-induced dislocations.

Kuroi et al. (221) found that more Cu is gettered to boron implants than to silicon implants. However, their I–V measurements indicate the silicon implants are more effective in reducing leakage currents with intentional Cu and Fe contamination. These results are in contradiction with the results of Benton et al. (229), who show that boron implants getter more Fe than silicon implants. The work of Benton et al. additionally shows that carbon is only moderately effective in gettering Fe, with a gettering effectiveness between that of boron and silicon implants. Their data for carbon gettering are in agreement with Skorupa et al. (227) with respect to residual dissolved Fe in the near-surface region.

Overwijk et al. (228) present results on implantation gettering of Fe and Cu that show that carbon and oxygen implantation gettering is active at implant doses below 6×10^{15} at./cm^2 but He implantation is not. However, at doses greater than 6×10^{15} at./cm^2, the He implantation getters significantly more impurities than carbon or oxygen.

Seidel et al. (163) have determined that gettering of Au varies with implant species, the order of effectiveness being $\mathrm{Ar} \geq \mathrm{O} > \mathrm{P} > \mathrm{Si} > \mathrm{As} \geq \mathrm{B}$, with all species implanted at 200 keV and at a dose of 10^{16} at./cm^2. However, in all of the above comparisons one must consider the annealing temperature, which can significantly affect gettering to the P, As, B, H, and He implants, due to the temperature dependence of segregation gettering. Additionally, the cooling conditions or degree of supersaturation must be considered, since this can drastically change the gettering effectiveness of nondopant implant species (e.g. Ar, O, and Si), which getter by a relaxation mechanism.

A comparison between gettering to He-implantation-induced cavities and to internal gettering sites has been made by McHugo et al. (233,235) for Cu and Fe. Their results indicate that the majority of impurities are gettered to the cavities and that impurities are removed from the device region faster with cavities than with internal gettering sites. The increased gettering kinetics is likely due to the close proximity of the cavities to the device region and the fact that gettering to cavities occurs even without an impurity supersaturation.

A drawback of gettering by implantation is that implantation-induced defects can degrade device performance. Of particular concern is the increase in concentrations of native point defects, vacancies, and self-interstitials, which can enhance dopant diffusion in the device region and hinder shallow-junction formation (245). This problem may be alleviated with coimplantation of carbon, which has been shown to inhibit dynamic annealing of implant damage (246). The carbon implant essentially captures self-interstitials, as has been shown previously in electron irradiation work (247). Another drawback is the requisite high implant doses, which correspond to undesirably long implantation times. However, rapid implantation of many species has been shown using plasma

immersion ion implantation, where a typical implantation of 2×10^{17} H/cm^2 takes on the order of 2 min (248).

GETTERING SIMULATIONS

The fundamental phenomena of gettering is the diffusion of impurities which is described by Fick's diffusion equation. This parabolic differential equation can be easily implemented in an explicit or implicit finite differences algorithm which discretizes time, Δt, and spatial dimensions, Δx. Explicit finite differences are limited in speed by a stability criterion which does not exist for the implicit finite differences algorithm (see, for example, Refs. (249–252)). While the implicit formulation is stable for any size time step, Δt, larger errors are incurred with larger step sizes. The diffusivity of metals in silicon are temperature dependent and decrease during a slow cool. Additionally, *effective* diffusion coefficients are functions of the metal concentrations themselves (46,90). Thus it is obvious that a changing diffusion coefficient must also be taken into account when modeling gettering. Within this finite differences algorithm, the gettering mechanisms, relaxation and segregation, are then included. For relaxation gettering, Ham's law (68) is used to model the precipitation of the impurity. For segregation, there exist a few different approaches, all of which modify the diffusion equation directly.

Modeling Relaxation Gettering Based on the Growing Radius Solution

Taking into account the growth of the precipitates and the increase of their radii during growth, Ham solved the three-dimensional diffusion equation and obtained the following analytical equation to describe the kinetics of precipitation:

$$Dt \cdot \left(\frac{4\pi n}{3}\right)^{2/3} \left(\frac{(c_0 - c_s)(1+Z)}{c_p - c_s}\right)^{1/3} = \frac{1}{6}\ln\left(\frac{[u(t)^2 + u(t) + 1][u(0)^2 - 2u(0) + 1]}{[u(t)^2 - 2u(t) + 1][u(0)^2 + u(0) + 1]}\right) - \frac{1}{\sqrt{3}}\tan^{-1}\left(\frac{2u(t)+1}{\sqrt{3}}\right) + \frac{1}{\sqrt{3}}\tan^{-1}\left(\frac{2u(0)+1}{\sqrt{3}}\right) \tag{20}$$

where

$$u(t)^3 = 1 - \frac{\overline{c}(t) - c_s}{[\overline{c}(0) - c_s](1+Z)} \quad \text{and} \quad Z = \frac{4\pi n r_0^3}{3} \cdot \frac{c_p - c_s}{c_0 - c_s} \tag{21}$$

and where $\overline{c}(t)$ is the time-dependent solute (impurity) concentration, c_0 is the initial impurity concentration, c_s is the impurity equilibrium solubility concentration, c_p is the density of the impurity in the precipitate, D is the diffusivity at the fixed precipitation temperature, n is the precipitate site density, and r_0 is the initial precipitate radius. It should be noted that if all the solute is dissolved at $t = 0$, then r_0 can be set to 0.

Equations (20) and (21) can be used to fit given experimental data on isothermal precipitation by varying n until a satisfactory fit is obtained. It has been used, for example, by Livingston et al. (253) to model the precipitation of oxygen in silicon. However, because of the implicit nature of this formulation, it is not useful in conjunction with computer simulation programs (e.g., finite-difference calculations) that model diffusion and other processes.

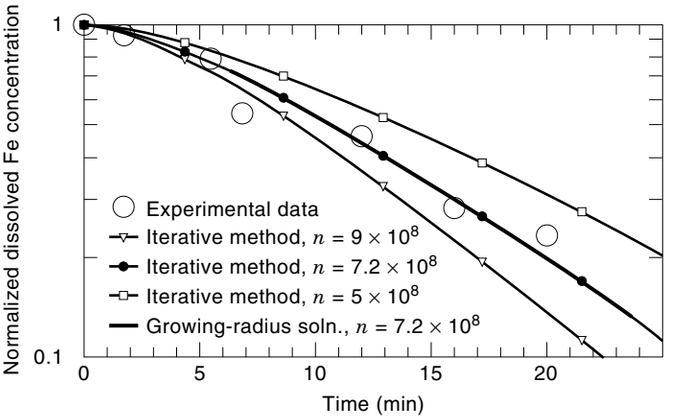

Figure 13. An example of the use of Ham's equations to obtain the precipitation site density n. The bold line is the exact analytic solution with a growing radius given by Ham using an iron precipitate density of 7.2×10^8 sites/cm^3. The iterative technique with the same site density yields the same curve. Variations in n are also plotted.

Modeling Relaxation Gettering Based on the Fixed Radius Solution

Using an iterative technique based on the fixed-radius solution provides several advantages. First, this method can simulate the growing-radius solution by appropriately increasing the radius after each small time interval Δt. Furthermore, this approach can be used in conjunction with other finite-difference simulations that require an explicit expression for the change in dissolved concentration as a function of time. Another important advantage is that precipitation can still be modeled when the radius, precipitate site density, or diffusivity are not fixed (see 85, 254). Tan et al. (255) has proposed the use of the following formulae for modeling of precipitation:

$$\frac{d\overline{c}}{dt} = 4\pi n r D(c_s - \overline{c}) \tag{22}$$

and r is determined by an equation obtained by Ham,

$$\frac{dr}{dt} = c_p D \frac{\overline{c} - c_s}{r} \tag{23}$$

In the iterative method, r_0 cannot be set to 0 at the start of these simulations in the same manner as in the analytical solution, otherwise, if it is, no precipitation will result. This is because Ham's law does not take nucleation into account. Thus, at the start of the simulation, r_0 should be initially set to a very small value, such as the nucleus capture radius. While the initial choice of r_0 may at first appear problematic, the final solution does not depend significantly on it as long as it is small.

Thus Ham's equations can be used to quantify precipitation rates in terms of n and r_0. Experimental data can be fitted and quantified. An example of iron precipitation in Cz silicon with no oxygen precipitates is shown in Fig. 13. The

precipitation sites themselves are unknown but are suspected to be grown in defects.

Modeling more complex precipitation behavior, such copper precipitation, is difficult. There may, however, be several simplifications that allow simulations of copper precipitation, and thus of relaxation gettering of copper. One simplification is to use an effective silicide density, which would amount to treating the precipitate colony as one large precipitation site.

Computer Modeling of Segregation

Tan et al. (255,256) described the equations for modeling segregation. The equations were derived from thermodynamic considerations. Thus, segregation is a result of a gradient in the chemical potential which is included in the flux term in much the same manner as an electrical potential would be included for charged particles. The general flux and diffusion–segregation equations are as follows:

$$J = -D\left(\frac{\partial C}{\partial x} - \frac{C}{m}\frac{\partial m}{\partial x}\right) \tag{24}$$

and

$$\frac{\partial C}{\partial t} = \frac{\partial}{\partial x}\left[D\left(\frac{\partial C}{\partial x} - \frac{C}{m}\frac{\partial m}{\partial x}\right)\right] \tag{25}$$

where J is the flux of impurities, C is the impurity concentration, x is the spatial coordinate, D is the diffusivity of the impurity, and m is the segregation coefficient defined as

$$m = \frac{C^{\text{eq}}(x)}{C^{\text{eq}}(\text{ref})} \tag{26}$$

where $C^{\text{eq}}(x)$ is the equilibrium solubility at x and $C^{\text{eq}}(\text{ref})$ is the equilibrium solubility at some reference point in the crystal region. This approach has the disadvantage, when treating abrupt interfaces, that the interface must be approximated with a large number of nodes.

A simple approach was proposed by Antoniadis and Dutton (257), who modified the flux term to

$$J_{\text{seg}} = h\left(C_n - \frac{C_{n+1}}{m}\right) \tag{27}$$

where J_{seg} is the impurity segregation flux across the interface, and h is a mass transfer coefficient. The subscripts on the concentration designate the node. Thus C_n is the concentration of the node before the interface, and $C_{n+}1$ is the first node on the other side of the interface. This approach essentially manipulates a kinetic equation to simulate segregation, a thermodynamic phenomenon. Tan argues that while the modification of the gradient was a valid approach, the choice of h is problematic and depends upon the method used. Hieslmair et al. (31) used a similar expression,

$$J_{\text{seg}} = \frac{D_{\text{eff}}}{\Delta x}\left(C_n - \frac{C_{n+1}}{m}\right) \tag{28}$$

where

$$D_{\text{eff}} = \frac{D_n D_{n+1}}{D_n + D_{n+1}} \tag{29}$$

The factor D_{eff} is important when the diffusivity of the impurity changes across the interface. This term assumes the interface to be halfway between nodes n and $n + 1$ and essentially provides the effective rate-limiting diffusion coefficient. This equation, however, works only for segregation of impurities from n to $n + 1$, that is, $m > 1$. For segregation in the opposite direction, C_n should be divided by m. In general, this approach of modifying the concentration gradient provides satisfactory results.

The major difficulty with gettering simulations is to accurately obtain the material parameters such as n, r_0, the segregation coefficient, and sometimes even the diffusivity. Additionally, it remains to be seen whether these simple models can satisfactorily model gettering considering that some impurities exhibit complex gettering behaviors and defect interactions.

BIBLIOGRAPHY

1. E. R. Weber, Transition Metals in Silicon, *Appl. Phys. A,* **30**: 1, 1983.
2. H. Lemke, in *Fourth International Symposium on High Purity Silicon,* C. L. Claeys et al. (eds.), San Antonio, TX: Electrochemical Society, Vol. 96-13, 1996, p. 272.
3. R. F. Pierret, *Semiconductor Device Fundamentals,* Reading, MA: Addison-Wesley, 1996.
4. O. V. Bogorodskii et al., Mechanisms for the decreased breakdown voltage in high-voltage multilayer silicon thyristors, *Zhurnal Tekhnicheskoi Fiziki,* **55**: 1419–1425, 1985.
5. L. K. J. Vandamme et al., Impact of silicon substrate, iron contamination and perimeter on saturation current and noise in n/sup +/p diodes, *Solid-State Electron.,* **41**: 901–908, 1997.
6. H. H. Busta and H. A. Waggener, Precipitation-induced currents and generation-recombination currents in intentionally contaminated silicon P/sup +/N junctions, *J. Electrochem. Soc.,* **124**: 1424–1429, 1977.
7. W. Schröter et al., Bandlike and localized states at extended defects in silicon, *Phys. Rev. B,* **52**: 13726, 1995.
8. A. A. Istratov et al., in *Defect & Impurity Engineered Semiconductors & Devices II,* S. Ashok et al. (eds.), San Francisco, CA: Materials Research Society, Vol. 510, 1998.
9. B. O. Kolbesen et al., Impact of defects on the technology of highly integrated circuits, *Mater. Sci. Forum,* **38–41**: 1–12, 1989.
10. L. Jastrzebski, Origin and control of material defects in silicon, *IEEE Trans. Electron Dev.,* **ED-29**: 475, 1982.
11. P. J. Ward, A survey of iron contamination in silicon substrates and its impact on circuit yield, *J. Electrochem. Soc.,* **129**: 2573–2576, 1982.
12. J. C. Lee et al., Modeling and characterization of gate oxide reliability, *IEEE Trans. Electron Dev.,* **35**: 2269, 1988.
13. K. Honda et al., Behavior of Fe impurity during HCl oxidation, *J. Electrochem. Soc.,* **142**: 3486, 1995.
14. A. Ohsawa et al., Metal impurities near the SiO/sub 2/-Si interface, *J. Electrochem. Soc.,* **131**: 2964–2969, 1984.
15. R. Falster, in *Crystalline Defects and Contamination: Their Impact and Control in Device Manufacturing,* B. O. Kolbesen et al. (eds.), Grenoble, France: Electrochemical Society, Vol. 93-15, 1993, p. 149.
16. P. W. Mertens et al., in *Crystalline Defects and Contamination: Their Impact and Control in Device Manufacturing,* B. O. Kolbesen et al. (eds.), Grenoble, France: Electrochemical Society, Vol. 93-15, 1993, p. 87.

17. F. Tardif et al., in *Crystalline Defects and Contamination: Their Impact and Control in Device Manufacturing,* B. O. Kolbesen et al. (eds.), Grenoble, France: Electrochemical Society, Vol. 93-15, 1993, p. 114.
18. K. Honda and T. Nakanishi, Influence of Ni impurities at the Si-SiO2 interface on the metal-oxide-semiconductor characteristics, *J. Appl. Phys.,* **75**: 7394, 1994.
19. K. Honda et al., Catastrophic breakdown in silicon oxides: the effect of Fe impurities at the SiO/sub 2/-Si interface, *J. Appl. Phys.,* **62**: 1960–1963, 1987.
20. K. Honda et al., Breakdown in silicon oxides (II)-correlation with Fe precipitates, *Appl. Phys. Lett.,* **46**: 582–584, 1985.
21. K. Honda et al., Breakdown in silicon oxides-correlation with Cu precipitates, *Appl. Phys. Lett.,* **45**: 270–271, 1984.
22. K. Hiramoto et al., Degradation of gate oxide integrity by metal impurities, *Jpn. J. Appl. Phys., Part 2* (Letters), **28**: L2109–L2111, 1989.
23. W. B. Henley et al., The effects of iron contamination on thin oxide breakdown: experimental and modeling, in *Defect Engineering in Semiconductor Growth, Processing and Device Technology,* S. Ashok et al. (eds.), San Francisco, CA: Materials Research Society, 1992, pp. 993–998.
24. R. Takizawa et al., Degradation of metal-oxide-semiconductor devices caused by iron impurities on the silicon wafer surface, *J. Appl. Phys.,* **62**: 4933–4935, 1987.
25. W. Rieger, in *Crystalline Defects and Contamination: Their Impact and Control in Device Manufacturing,* B. O. Kolbesen et al. (eds.), Grenoble, France: Electrochemical Society, Vol. 93-15, 1993, p. 103.
26. W. C. McColgin et al., Deep level traps in CCD Image Sensors, in *Defect & Impurity Engineered Semiconductors & Devices II,* S. Ashok et al. (eds.), San Francisco, CA: Materials Research Society, 1998, in print.
27. A. Rohatgi et al., Opportunities in silicon Photovoltaics and Defect Control in Photovoltaic Materials, *J. Electron. Mater.,* **22**: 65–72, 1993.
28. S. A. McHugo et al., Gettering of metallic impurities in photovoltaic silicon, *Appl. Phys. A,* (Materials Science Processing), **A64**: 127–137, 1997.
29. B. Sopori, in *Defect & Impurity Engineered Semiconductors & Devices II,* S. Ashok et al. (eds.), San Francisco, CA: Materials Research Society, 1998, in print.
30. H. Hieslmair et al., Aluminum Gettering and Transition Metal Precipitates in PV Silicon, in *NREL/SNL Photovoltaics Program Review,* C. E. Witt et al. (eds.), Lakewood, CO: AIP Conf. Proc., Vol. 394, 1996, p. 759.
31. S. M. Joshi et al., Improvement of minority carrier diffusion length in Si by Al gettering, *J. Appl. Phys.,* **77**: 3858–3863, 1995.
32. P. Sana et al., Gettering and hydrogen passivation of edge-defined film-fed grown multicrystalline silicon solar cells by Al diffusion and forming gas anneal, *Appl. Phys. Lett.,* **64**: 97–99, 1994.
33. A. Rohatgi et al., Effect of titanium, copper and iron on silicon solar cells, *Solid-State Electron.,* **23**: 415–422, 1980.
34. F. Secco d'Aragona et al., Effect of impurity gettering on the efficiency of metallurgical-grade silicon solar cells, *Solar Cells,* **10**: 129–143, 1983.
35. M. Hourai et al., Behavior of defects induced by metallic impurities on Si(100) surfaces, *Jpn. J. Appl. Phys., Part 1* (Regular Papers & Short Notes), **28**: 2413–2420, 1989.
36. B. Shen et al., Influences of Cu and Fe impurities on oxygen precipitation in Czochralski-grown silicon, *Jpn. J. Appl. Phys., Part 1,* **35**: 4187–4194, 1996.
37. H. Mikoshiba et al., Defect analyses in VLSI devices by TEM observations and process simulation, in *Defect Engineering in Semiconductor Growth, Processing, and Device Technology,* S. Ashok et al. (eds.), San Francisco, CA: Materials Research Society, 1992, pp. 629–639.
38. The National Technology Roadmap for Semiconductors, in *The National Technology Roadmap for Semiconductors,* San Jose, CA: Semiconductor Industry Association, 1994, pp. 110–113.
39. R. B. M. Girisch, in *Crystalline Defects and Contamination: Their Impact and Control in Device Manufacturing,* B. O. Kolbesen et al. (eds.), Grenoble, France: Electrochemical Society, Vol. 93–15, 1993, p. 170.
40. A. Shah and P. Yang, MOS Technology: Trends and Challenges in the ULSI Era, *Microelectron. Reliab.,* **37**: 1301, 1995.
41. W. H. Krautschneider et al., Scaling Down and Reliability Problems of Gigabit CMOS Circuits, *Microelectron. Reliab.,* **37**: 19, 1997.
42. J. S. Kang and D. K. Schroder, Gettering in Silicon, *J. Appl. Phys.,* **65**: 2974–2985, 1989.
43. S. A. McHugo, Release of metal impurities from structural defects in polycrystalline silicon, *Appl. Phys. Lett.,* **71**: 1984, 1997.
44. W. Schröter et al., in *Electronic Structure and Properties of Semiconductors,* R. W. Cahn et al. (eds.), Weinheim: VCH, 1991, p. 539.
45. H. Reiss, Chemical effects due to the ionization of impurities in semiconductors, *J. Chem. Phys.,* **21**: 1209, 1953.
46. H. Reiss et al., Chemical Interactions Among Defects in Germanium and Silicon, *The Bell Syst. Tech. J.,* **35**: 535, 1956.
47. W. Shockley and J. T. Last, Statistics of the charge distribution for a localized flaw in a semiconductor, *Phys. Rev.,* **107**: 392, 1957.
48. W. Shockley and J. L. Moll, Solubility of Flaws in Heavily-Doped Semiconductors, *Phys. Rev.,* **119**: 1480, 1960.
49. H. Lemke, Dotierungseigenschaften von Eisen in Silizium, *Phys. Status Solidi A,* **64**: 215, 1981.
50. L. C. Kimerling and J. L. Benton, Electronically controlled reactions of interstitial iron in silicon, *Physica B & C,* **116B**: 297–300, 1983.
51. L. Chantre and D. Bois, Metastable-defect behavior in silicon: Charge-state-controlled reorientation of iron-aluminum pairs, *Phys. Rev. B,* **31**: 7979, 1985.
52. G. L. Campisi et al., A SiGe strain layer for gettering Fe in SIMOX, in *Proceedings of 1993 IEEE International SOI Conference,* Palm Springs, CA: IEEE, 1993, p. 56.
53. A. Ihlal et al., Correlation between the gettering efficiencies and the energies of interfaces in silicon bicrystals, *J. Appl. Phys.,* **80**: 2665, 1996.
54. S. A. McHugo et al., A Study of Gettering Efficiency and Stability in Czochralski Silicon, *Appl. Phys. Lett.,* **66**: 2840, 1995.
55. R. N. Hall and J. H. Racette, Diffusion and solubility of copper in extrinsic and intrinsic germanium, silicon and gallium arsenide, *J. Appl. Phys.,* **35**: 379, 1964.
56. D. Gilles et al., Impact of the electronic structure on the solubility and diffusion of 3d transition metals in silicon, *Phys. Rev. B,* **41**: 5770–5782, 1990.
57. P. A. Stolk et al., The Mechanism of Iron Gettering in Boron-Doped Silicon, *Appl. Phys. Lett.,* **68**: 51, 1996.
58. S. A. McHugo et al., Iron Solubility in Highly Boron-Doped Silicon, *Appl. Phys. Lett.,* (to be published Sept. 7, 1998).
59. J. D. McBrayer et al., Diffusion of Metals in Silicon Dioxide, *J. Electrochem. Soc.,* **133**: 1242, 1986.
60. J. Utzig, An elastic energy approach to the interstitial diffusion of 3d elements in silicon, *J. Appl. Phys.,* **65**: 3868, 1989.

61. K. Masuda-Jindo, Electronic Theory of Gettering and Passivation of Impurities in Semiconductors, in *Defect Engineering in Semiconductor Growth, Processing and Device Technology,* S. Ashok et al. (eds.), San Francisco, CA: Materials Research Society, Vol. 262, 1992, p. 999.
62. W. Kaiser, *Phys. Rev.,* **105**: 1751, 1957.
63. E. J. Mets, Poisoning and Gettering Effects in Silicon Junctions, *J. Electrochem. Soc.,* **112**: 420, 1965.
64. T. Y. Tan et al., Intrinsic gettering by oxide precipitate induced dislocations in Czochralski Si, *Appl. Phys. Lett.,* **30**: 175, 1977.
65. G. A. Rozgonyi and C. W. Pearce, Gettering of surface and bulk impurities in Czochralski silicon wafers, *Appl. Phys. Lett.,* **32**: 747, 1978.
66. R. Sawada et al., Mechanical Damage Gettering Effect in Si, *Jpn. J. Appl. Phys.,* **20**: 2097, 1981.
67. M. C. Chen and V. J. Silvestri, Post-Epitaxial Polysilicon and Si3N4 Gettering in Silicon, *J. Electrochem. Soc.,* **129**: 1294, 1982.
68. F. S. Ham, Theory of Diffusion-Limited Precipitation, *J. Phys. Chem. Solids,* **6**: 335–351, 1958.
69. M. Miyazaki et al., Dependence of gettering efficiency on metal impurities, *Jpn. J. Appl. Phys., Part 2* (Letters), **28**: L519–L521, 1989.
70. M. S. Goorsky et al., The contrastive behavior of Fe and Cr during the intrinsic gettering of silicon, *J. Appl. Phys.,* **64**: 6716–6720, 1988.
71. K. Graff et al., Palladium-test: a tool to evaluate gettering efficiency, in *Impurity Diffusion and Gettering in Silicon,* R. B. Fair et al. (eds.), Boston, MA: Materials Research Society, 1985, pp. 19–24.
72. K. Graff et al., Monitoring of internal gettering during bipolar processes, *J. Electrochem. Soc.,* **135**: 952–957, 1988.
73. R. Falster and W. Bergholz, The Gettering of Transition Metals by Oxygen-Related Defects in Silicon, *J. Electrochem. Soc.,* **137**: 1548, 1990.
74. M. Seibt and K. Graff, Characterization of haze forming precipitates in silicon, *J. Appl. Phys.,* **63**: 4444, 1988.
75. D. Gilles et al., Mechanism of Internal Gettering of Interstitial Impurities in Czochralski-Grown Silicon, *Phys. Rev. Lett.,* **64**: 196, 1990.
76. R. Falster et al., Gettering and Gettering Stability of Metals at Oxide Particles in Silicon, in *Defect Engineering in Semiconductor Growth, Processing and Device Technology,* S. Ashok et al. (eds.), San Francisco, CA: Materials Research Society, Vol. 262, 1992, pp. 945–956.
77. B. Shen et al., Gettering of copper by bulk stacking faults and punched-out dislocations in Czochralski-grown silicon, *J. Appl. Phys.,* **76**: 4540–4546, 1994.
78. B. Shen et al., Precipitation of Cu, Ni, and Fe on Frank-Type Partial Dislocations in Czochralski-Grown Silicon, *Phys. Status Solidi A,* **155**: 321, 1996.
79. B. Shen et al., Precipitation of Cu and Fe in Dislocated Floating-Zone-Grown Silicon, *Jpn. J. Appl. Phys. Lett.,* **35**: 3301–3305, 1996.
80. B. Shen et al., Gettering of Fe Impurities by Bulk Stacking Faults in Czochralski-Grown Silicon, *Appl. Phys. Lett.,* **70**: 1876, 1997.
81. R. J. Falster et al., Gettering thresholds for transition metals by oxygen related defects in silicon, *Appl. Phys. Lett.,* **59**: 809, 1991.
82. Z. Laczik et al., Gettering of Copper and Nickel in Czochralski silicon by oxide particles: dependence on oxide particle density and cooling rate, *Solid State Phenom.,* **19&20**: 39, 1991.
83. S. Kusanagi et al., Electrical activity of extended defects and gettering of metallic impurities in silicon, *Mater. Sci. Technol.,* **11**: 685, 1995.
84. H. Hieslmair et al., Gettering of iron by oxygen precipitates, *Appl. Phys. Lett.,* **72**: 1460–1462, 1998.
85. H. Hieslmair et al., Analysis of iron precipitation in silicon as a basis for gettering simulations, in *Semiconductor Silicon,* H. Huff et al. (eds.), San Diego, CA: Electrochemical Society, Vol. PV-98-1, 1998, p. 1126.
86. L. Baldi et al., Heavy Metal Gettering in Silicon-Device Processing, *J. Electrochem. Soc.,* **127**: 164–169, 1980.
87. F. G. Kirscht et al., Strain and gettering in epitaxial silicon wafers, *Diffus. Defect Data B, Solid State Phenom.,* **56–57**: 355–363, 1997.
88. K. Sumino et al., Science of defect control in semiconductors, *Mater. Sci. Technol.,* **11**: 657–664, 1995.
89. J. W. Cahn, Nucleation on Dislocations, *Acta Metall.,* **5**: 169–172, 1957.
90. A. A. Istratov et al., Intrinsic diffusion coefficient of interstitial copper in silicon, *Phys. Rev. Lett.,* **81** (6): 1243–1246, 1998.
91. V. Higgs et al., Characterization of Dislocations in the Presence of Transition Metal Contamination, *Mater. Sci. Forum,* **83–87**: 1309, 1992.
92. M. Kittler et al., Influence of copper contamination on recombination activity of misfit dislocations in SiGe/Si epilayers: temperature dependence of activity as a marker characterizing the contamination level, *J. Appl. Phys.,* **78**: 4573, 1995.
93. P. R. Wilshaw and T. S. Fell, Electron Beam Induced Current Investigations of Transition Metal Impurities at Extended Defects in Silicon, *J. Electrochem. Soc.,* **142**: 4298, 1995.
94. J. Vanhellemont and C. Claeys, On the role of point defects in gettering processes, *Mater. Sci. Forum,* **38-41**: 171, 1989.
95. M. Seibt, Homogeneous and Heterogeneous precipitation of copper in silicon, in *Proceedings of the Sixth International Symposium on Silicon Materials Science and Technology: Semiconductor Silicon 1990,* H. R. Huff et al. (eds.), Vol. 90, 1990, p. 663.
96. *Semiconductors and Semimetals,* F. Shimura et al. (eds.), New York: Academic Press, Vol. 42, 1994.
97. H. Tsuya et al., Improved intrinsic gettering technique for high-temperature-treated CZ silicon wafers, *Jpn. J. Appl. Phys.,* **20**: L31–L34, 1981.
98. G. F. Cerofolini and M. L. Polignano, A comparison of gettering techniques for very large scale integration, *J. Appl. Phys.,* **55**: 579–585, 1984.
99. R. A. Craven and H. W. Korb, Internal gettering in silicon, *Solid State Technol.,* **24**: 55–61, 1981.
100. R. B. Swaroop, Advances in silicon technology for the semiconductor industry, II, *Solid State Technol.,* **26**: 97–101, 1983.
101. S. Kishino et al., A defect control technique for the intrinsic gettering in silicon device processing, *Jpn. J. Appl. Phys., Part 2* (Letters), **23**: L9–L11, 1984.
102. J. O. Borland, Borland's overview of the latest in intrinsic gettering, I, *Semiconductor Int.,* **12**: 144–148, 1989.
103. L. Jastrzebski et al., A comparison of internal gettering during bipolar, CMOS, and CCD (high, medium, low temperature) processes, *J. Electrochem. Soc.,* **134**: 1018–1025, 1987.
104. L. A. Cerra and H. Chiou, Effects of intrinsic gettering on RAM corruption and device yield of a CMOS process, in *Semiconductor Silicon,* H. R. Huff et al. (eds.), Electrochemical Society, 1994, p. 884.
105. F. G. Kirscht, Gettering phenomena in Epitaxial Silicon Structures, in *Semiconductor Silicon,* H. R. Huff et al. (eds.), Electrochemical Society, 1994, pp. 831–843.

106. R. Falster et al., The Engineering of Silicon Wafer Material Properties Through Vacancy Concentration Profile Control and the Achievement of Ideal Oxygen Precipitation Behavior, in *Defect & Impurity Engineered Semiconductors & Devices II,* S. Ashok et al. (eds.), San Francisco, CA: Materials Research Society, 1998, in print.
107. M. Seibt, Metal Impurity Precipitation in Silicon, in *Crystalline Defects and Contamination: Their Impact and Control in Device Manufacturing II,* B. O. Kolbesen et al. (eds.), Pennington, NJ: Electrochem. Society, Vol. PV 97-22, 1997, p. 243.
108. A. A. Istratov and E. R. Weber, Electrical properties and recombination activity of copper, nickel and cobalt in silicon, *Appl. Phys. A,* **A66**: 123–136, 1998.
109. M. Ronay and R. G. Schad, New insight into silicide formation: the creation of silicon self-interstitials, *Phys. Rev. Lett.,* **64**: 2042, 1990.
110. S. Krieger-Kaddour et al., Transmission electron microscopic study of the morphology of oxygen precipitates and of chromium precipitation during intrinsic gettering in Czochralski-grown silicon: influence of lamp pulse annealings, *J. Electrochem. Soc.,* **140**: 495–500, 1993.
111. D. Gilles et al., Model of internal gettering from low-temperature Fe precipitation kinetics in Czochralski silicon, in *Proceedings of the Sixth International Symposium on Silicon Materials Science and Technology: Semiconductor Silicon 1990,* H. R. Huff et al. (eds.), Ibaraki-ken, Japan: Electrochemical Society, Vol. 90-7, 1990, p. 697.
112. A. R. Bhatti et al., TEM studies of the gettering of copper, palladium and nickel in Czochralski silicon by small oxide precipitates, *Gettering and defect engineering in semiconductor technology* (GADEST), 1991, pp. 51–56.
113. W. C. Dash, *J. Appl. Phys.,* **27**: 1193, 1956.
114. E. Nes, The Mechanism of Repeated Precipitation on Dislocations, *Acta Metall.,* **22**: 81, 1974.
115. E. Nes and J. Washburn, Precipitate colonies in silicon, *J. Appl. Phys.,* **42**: 3562, 1971.
116. J. K. Solberg and E. Nes, The interaction between vacancy emitting/absorbing precipitates and dislocations in silicon as investigated by transmission electron microscopy, *Philos. Mag. A,* **37**: 465–478, 1978.
117. M. Seibt, On the role of stacking faults in copper precipitation in silicon, *Gettering and defect engineering in semiconductor technology (GADEST),* 1991, pp. 45–50.
118. S. Sadamitsu et al., Gettering in advanced low temperature processes, *Diffus. Defect Data B, Solid State Phenom.,* **57–58**: 53–62, 1997.
119. L. Fabry et al., Reaction path of internal gettering of iron in semiconductor silicon, *Jpn. J. Appl. Phys. 1,* **33**: 510–513, 1994.
120. B. Hackl et al., Correlation between DLTS and TRXFA measurements of copper and iron contaminations in FZ and CZ silicon wafers; application to gettering efficiencies, *J. Electrochem. Soc.,* **139**: 1495–1498, 1992.
121. G. E. J. Eggermont et al., Laser Induced Backside Damage Gettering, *Solid State Technol.,* **26**: 171, 1983.
122. R. Sawada, Durability of Mechanical Damage Gettering Effect in Si Wafers, *Jpn. J. Appl. Phys.,* **23**: 959, 1984.
123. Y. Hayamizu et al., Impurity gettering in silicon by thin polycrystalline films, in *Defect Engineering in Semiconductor Growth, Processing and Device Technology,* S. Ashok et al. (eds.), San Francisco, CA: Materials Research Society, Vol. 262, 1992, p. 1005.
124. S. Ogushi et al., Gettering characteristics of heavy metal impurities in silicon wafers with polysilicon back seal and internal gettering, *Jpn. J. Appl. Phys.,* Part 1 (Regular Papers, Short Notes, & Review Papers) **36**: 6601–6606, 1997.
125. D. Gilles, Mechanisms of transition element gettering in silicon, in *Defect Engineering in Semiconductor Growth, Processing and Device Technology,* S. Ashok et al. (eds.), San Francisco, CA: Materials Research Society, Vol. 262, 1992, p. 917.
126. D. Gilles and H. Ewe, Gettering phenomena in silicon, in *Semiconductor Silicon,* H. R. Huff et al. (eds.), San Francisco, CA: Electrochemical Society, 1994, pp. 772–783.
127. M. Seibt et al., Modeling and experimental verification of gettering mechanisms, in *Semiconductor Silicon,* H. Huff et al. (eds.), San Diego, CA: Electrochemical Society, Vol. PV–98–1, 1998, p. 1064.
128. Y. Hayamizu et al., Computer simulation of impurity gettering capability in silicon for current gettering techniques, in *Semiconductor Silicon,* H. Huff et al. (eds.), San Diego, CA: Electrochemical Society, Vol. PV–98–1, 1998, p. 1080.
129. K. Sumino, Current problems of defects in semiconductors—interaction of defects with impurities, *Mater. Sci. Forum,* **105-110**: 139, 1992.
130. H. Shirai et al., Effect of back-surface polycrystalline silicon layer on oxygen precipitation in Czochralski silicon wafers, *Appl. Phys. Lett.,* **54**: 1748, 1989.
131. K. K. Mishra, Mechanism of iron gettering by polycrystalline silicon film in *p*-type Czochralski silicon, in *Defect and Impurity Engineered Semiconductors and Devices, MRS Symposium,* S. Ashok et al. (eds.), San Francisco: Materials Research Society, 1995, p. 321.
132. V. V. Voronkov, Generation of thermal donors in silicon: oxygen aggregation controlled by self-interstitials, *Semicond. Sci. Technol.,* **8**: 2037, 1993.
133. M. B. Shabani et al., A Quantitative Method of Metal Impurities Depth Profiling for Gettering Evaluation in Silicon Wafers, *Diffus. Defect Data, Part B, Solid State Phenom.,* **57–58**: 81, 1997.
134. S. J. Brunkhorst and D. W. Sloat, The impact of the 300-mm transition on silicon wafer suppliers, *Solid State Technol.,* **41**: 87, 1998.
135. H. Hieslmair et al., Aluminum backside segregation gettering, in *25th IEEE Photovoltaic Specialists Conference,* Washington, DC: IEEE, 1996, pp. 441–444.
136. S. A. McHugo et al., Gettering in Multicrystalline Silicon, in *International Conference on Defects in Semiconductors, Materials Science Forum,* M. Suezawa and H. Katayama-Yoshida (eds.), Sendai, Japan: Trans Tech Publications, Vol. 196–201, 1995, p. 1979.
137. L. A. Verhoef et al., Gettering in polycrystalline silicon solar cells, *Mater. Sci. Eng. B,* **B7**: 49–62, 1990.
138. I. Périchaud et al., Phosphorus external gettering efficiency in multicrystalline silicon, in *Gettering Defect Eng. Semicond. Technol. (GADEST '93),* Chossewitz, Germany: Vol. 32–33, 1993, pp. 77–82.
139. K. Mahfoud et al., Influence of carbon and oxygen on phosphorus and aluminum co-gettering in silicon solar cells, *Mater. Sci. Eng. B,* **36**: 63–67, 1996.
140. R. R. Troutman, Epitaxial layer enhancement of n-well guard rings for CMOS circuits, *IEEE Electron Devices Lett.,* **EDL-4**: 438, 1983.
141. S. F. Cagnina, Enhanced gold solubility effect in heavily n-type silicon, *J. Electrochem. Soc.,* **116**: 498, 1969.
142. T. A. O'Shaughnessy et al., The solid solubility of gold in doped silicon by oxide encapsulation, *J. Electrochem. Soc.,* **121**: 1350, 1974.
143. R. W. Gregor and J. W. H. Stinebaugh, Studies of effective gettering techniques using segregation annealing for complementary metal-oxide-semiconductor technologies, *J. Appl. Phys.,* **64**: 2079, 1988.

144. G. F. Cerofolini et al., The role of dopant and segregation annealing in silicon p-n junction gettering, *Phys. Status Solidi A,* **103**: 643, 1987.

145. M. Sano et al., Gettering techniques of heavy metal impurities in silicon, in *Semiconductor Silicon 1994: Electrochem. Soc. Meeting,* Electrochemical Society, 1994, pp. 784–795.

146. M. Aoki et al., Gettering of iron impurities in p/p+ epitaxial silicon wafers with heavily boron-doped substrates, *Appl. Phys. Lett.,* **66**: 2709, 1995.

147. M. Aoki et al., Mo contamination in p/p+ epitaxial silicon wafers, *Jpn. J. Appl. Phys.,* **34**: 712, 1995.

148. M. Miyazaki et al., Efficiency of boron gettering for iron impurities in p/p/sup +/epitaxial silicon wafers, *Jpn. J. Appl. Phys.,* **36**, L380, 1997.

149. H. Tomita et al., Gettering of iron using electrically inactive boron doped layer, in *18th International Conference on Defects in Semiconductors, ICDS-18,* Sendai, Japan: Trans Tech Publications, 1995, Vol. 196–201, pp. 1991–1996.

150. H. Lemke, Energieniveaus und Bindungsenergien von Ionenpaaren in Silizium, *Phys. Status Solidi A,* **76**: 223, 1983.

151. D. P. Miller et al., *J. Appl. Phys.,* **33**: 2648, 1962.

152. M. L. Joshi and F. Wilhelm, *J. Electrochem. Soc.,* **112**: 185, 1965.

153. T. H. Yeh and M. L. Joshi, Strain compensation in silicon by diffused impurities, *J. Electrochem. Soc.,* **116**: 73, 1969.

154. H. Kikuchi et al., New gettering using misfit dislocations in homoepitaxial wafers with heavily boron-doped silicon substrates, *Appl. Phys. Lett.,* **54**: 463, 1989.

155. H. Tsuya et al., Behaviours of thermally induced microdefects in heavily doped silicon wafers, *Jpn. J. Appl. Phys.,* **22**: L16, 1983.

156. S. Matsumoto et al., Effect of dopant concentration on the growth of oxide precipitates in silicon, in *Materials Research Society,* R. B. Fair et al. (eds.), Boston, MA: Vol. 36, 1984, p. 263.

157. H. Takeno et al., Evaluation method of precipitated oxygen concentration in low resistivity silicon wafers using X-ray diffraction, in *18th International Conference on Defects in Semiconductors,* M. Suezawa and H. Katayama-Yoshida (eds.), Sendai, Japan: Trans Tech Publications, Vol. 196–201, 1995, p. 1865.

158. S. M. Myers et al., Strong segregation gettering of transition metals by implantation-formed cavities and boron-silicide precipitates in silicon, *Nucl. Instrum. Methods B,* **120**: 43, 1996.

159. W. R. Wilcox et al., Gold in silicon: Effect on resistivity and diffusion in heavily-doped layers, *J. Electrochem. Soc.,* **111**: 1377, 1964.

160. W. R. Wilcox and T. J. LaChapelle, Mechanism of gold diffusion into silicon, *J. Appl. Phys.,* **35**: 240, 1964.

161. M. L. Joshi and S. Dash, Distribution and precipitation of gold in phosphorus-diffused silicon, *J. Appl. Phys.,* **37**: 2453, 1966.

162. R. L. Meek and C. F. Gibbon, Preliminary results of an ion scattering study of phosphosilicate glass gettering, *J. Electrochem. Soc.,* **121**: 444, 1974.

163. T. E. Seidel et al., Direct comparison of ion-damage gettering and phosphorus-diffusion gettering of Au in Si, *J. Appl. Phys.,* **46**: 600, 1975.

164. R. L. Meek et al., Diffusion gettering of Au and Cu in silicon, *J. Electrochem. Soc.,* **122**: 786, 1975.

165. W. F. Tseng et al., Simultaneous gettering of Au in silicon by phosphorus and dislocations, *Appl. Phys. Lett.,* **33**, 442–444, 1978.

166. L. Baldi et al., Gold Solubility in Silicon and Gettering by Phosphorus, *Phys. Status Solid. A,* **48**: 523, 1978.

167. E. O. Sveinbjörnsson et al., Phosphorus diffusion gettering of gold in silicon: The reversibility of the gettering process, *J. Appl. Phys.,* **73**: 7311–7321, 1993.

168. E. Yakimov and I. Perichaud, Phosphorus diffusion effect on defect structure of silicon with oxygen precipitates revealed by gold diffusion study, *Appl. Phys. Lett.,* **67**: 2054–2056, 1995.

169. A. Ourmazd and W. Schröter, Phosphorus gettering and intrinsic gettering of nickel in silicon, *Appl. Phys. Lett.,* **45**: 781, 1984.

170. A. Goetzberger and W. Shockley, Metal precipitates in silicon p-n junctions, *J. Appl. Phys.,* **31**: 1821, 1960.

171. R. Kühnapfel and W. Schröter, Phosphorus diffusion gettering of cobalt in silicon: time development and critical behavior, in *Semiconductor Silicon '90,* H. R. Huff et al. (eds.), San Diego, CA: Electrochemical Society, 1990, p. 651.

172. W. Schröter and R. Kühnapfel, Model describing phosphorus diffusion gettering of transition elements in silicon, *Appl. Phys. Lett.,* **56**: 2207, 1990.

173. R. Falster, Platinum gettering in silicon by phosphorus, *Appl. Phys. Lett.,* **46**: 737, 1985.

174. H. Zimmermann et al., Pairing of noble metals with phosphorus, *Appl. Phys. Lett.,* **60**: 748, 1992.

175. G. J. Sprokel and J. M. Fairchild, Diffusion of gold into silicon crystals, *J. Electrochem. Soc.,* **112**: 200, 1965.

176. S. L. Chou and J. F. Gibbons, Study of the enhanced solubility and lattice location of gold impurities in a heavily-phosphorus-diffused layer of silicon, *J. Appl. Phys.,* **46**: 1197, 1975.

177. F. Gaiseanu and W. Schröter, Contribution of diffusion interstitial injection to gettering of metallic impurities in silicon, *J. Electrochem. Soc.,* **143**: 361–362, 1996.

178. E. Spiecker et al., Phosphorus-diffusion gettering in the presence of a nonequilibrium concentration of silicon interstitials: a quantitative model, *Phys. Rev. B,* **55**: 9577–9583, 1997.

179. A. Bourret and W. Schröter, HREM of SiP precipitates at the (111) silicon surface during phosphorus predeposition, *Ultramicroscopy,* **14**: 97, 1984.

180. B. Hartiti et al., Large diffusion length enhancement in silicon by rapid thermal codiffusion of phosphorus and aluminum, *Appl. Phys. Lett.,* **63**: 1249–1251, 1993.

181. J. J. Simon et al., Influence of phosphorus diffusion on the recombination strength of dislocations in float zone silicon wafers, *J. Appl. Phys.,* **80**: 4921, 1996.

182. S. Martinuzzi and I. Perichaud, Influence of oxygen on external phosphorus gettering in disordered silicon wafers, in *17th Int. Conf. on Defects in Semiconductors,* Gmunden, Austria: Materials Science Forum, 1994, Vol. 143–147, pp. 1629–1633.

183. M. Loghmarti et al., Strong improvement of diffusion length by phosphorus and aluminum gettering, *Appl. Phys. Lett.,* **62**: 979–981, 1993.

184. B. L. Sopori et al., Gettering effects in polycrystalline silicon, in *12th Eur. Photovoltaic Solar Energy Conf.,* The Netherlands, 1994, p. 1003.

185. L. Jastrzebski et al., Improvement of diffusion length in polycrystalline photovoltaic silicon by phosphorus and chlorine gettering, *J. Electrochem. Soc.,* **142**: 3869–3872, 1995.

186. M. L. Polignano et al., Gettering mechanisms in silicon, *J. Appl. Phys.,* **64**: 869–876, 1988.

187. R. Gafiteanu et al., Phosphorus and aluminum gettering of gold in silicon: simulation and optimization considerations, in *Defect Impurity Eng. Semicond. Devices, MRS Symp.,* S. Ashok et al. (eds.), San Francisco, 1995, pp. 297–302.

188. W. K. Schubert and J. M. Gee, Phosphorus and aluminum gettering—investigation of synergistic effects in single crystal and multicrystalline silicon, in *25th IEEE Photovoltaic Spec. Conf.,* Washington, DC: IEEE, 1996, pp. 437–440.

189. H. J. Queisser, *J. Appl. Phys.,* **32**: 1776, 1961.

190. M. Yoshida et al., Excess vacancy generation mechanism at phosphorus diffusion into silicon, *J. Appl. Phys.,* **45**: 1498, 1974.

191. R. B. Fair and J. C. C. Tsai, A quantitative model for the diffusion of phosphorus in silicon and the emitter dip effect, *J. Electrochem. Soc.,* **124**: 1107, 1977.
192. A. F. W. Willoughby, Interactions between sequential dopant diffusions in silicon—a review, *J. Phys. D,* **10**: 455, 1977.
193. A. Armigliato et al., On the Growth of Stacking Faults and Dislocations Induced in Si by Phosphorus Predeposition, *J. Appl. Phys.,* **48**: 1806, 1977.
194. H. Strunk et al., Interstitial Supersaturation near Phosphorus Diffused Emitter Zones, *Appl. Phys. Lett.,* **34**: 530, 1979.
195. H. Strunk et al., Interstitial supersaturation and climb of misfit dislocations in phosphorus-diffused silicon, *J. Microsc. (Oxford),* **118**: 35, 1980.
196. W. B. Knowlton et al., Properties of silicon point defects as revealed by lithium ion drifting, in *Electrochem. Soc. Meet.,* Los Angeles, CA: Electrochemical Society, 1996, p. 324.
197. U. Gösele et al., Mechanism and kinetics of the diffusion of gold in silicon, *Appl. Phys.,* **23**: 361, 1980.
198. U. Gösele et al., Diffusion of gold in silicon: A new model, *Appl. Phys. Lett.,* **38**: 157, 1981.
199. M. P. Godlewski et al., Low-High Junction Theory Applied to Solar Cells, in *10th IEEE Photovoltaic Spec. Conf.,* Palo Alto, CA: IEEE, 1973, p. 40.
200. J. Mandelkorn and J. Lamneck, A new electric field effect in silicon solar cells, *J. Appl. Phys.,* **44**: 4785, 1973.
201. R. Sundaresan et al., Potential improvement of polysilicon solar cells by grain boundary and intragrain diffusion of aluminum, *J. Appl. Phys.,* **55**: 1162–1167, 1984.
202. J. C. M. Hwang et al., Grain boundary diffusion of aluminum in polycrystalline silicon films, *J. Appl. Phys.,* **51**: 1576, 1980.
203. S. Martinuzzi et al., External gettering by aluminum-silicon alloying observed from carrier recombination at dislocations in float zone silicon wafers, *Appl. Phys. Lett.,* **70**: 2744–2746, 1997.
204. R. Janssens et al., Effects of grain boundary passivation in polycrystalline solar cells, in *15th IEEE Photovoltaics Spec. Conf.,* Kissimmee, FL: IEEE, 1981, pp. 1322–1325.
205. H. Fischer et al., Influence of controlled lifetime doping on ultimate technological performance of silicon solar cells, in *8th IEEE Photovoltaic Spec. Conf.,* Seattle, WA: IEEE, 1970, pp. 70–77.
206. C. F. Gay, Thin silicon solar cell performance characteristics, in *13th IEEE Photovoltaic Spec. Conf.,* Washington, DC: IEEE, 1978, p. 444.
207. R. Sundaresan et al., Improvement of polysilicon solar cells by aluminum diffusion, in *16th IEEE Photovoltaic Spec. Conf.,* San Diego, CA: IEEE, 1982, pp. 421–426.
208. W. A. Orr and M. Arienzo, Investigations of polycrystalline silicon back surface field solar cells, *IEEE Trans. Electron Devices,* **29**: 1151–1155, 1982.
209. R. D. Thompson and K. N. Tu, Low temperature gettering of Cu, Ag and Au across a wafer of Si by Al, *Appl. Phys. Lett.,* **41**: 440–442, 1982.
210. S. Martinuzzi et al., Influence of aluminum or copper diffusions on electronic properties of p-type cost polycrystalline silicon, in *18th IEEE Photovoltaic Spec. Conf.,* Las Vegas, NV: IEEE, 1985, pp. 1127–1132.
211. S. Martinuzzi et al., Improvement of electron diffusion lengths in polycrystalline silicon wafers by aluminum, *Rev. Phys. Appl.,* **22**: 645–648, 1987.
212. M. L. Rock et al., Process induced improvements in polycrystalline silicon-film solar cells, in *21st IEEE Photovoltaic Spec. Conf.,* Kissimmee, FL, Vol. 1, 1990, p. 1673.
213. N. Gay and S. Martinuzzi, Comparison of external gettering efficiency of phosphorus diffusion, aluminum-silicon alloying and helium implantation in silicon wafers, in *Gettering Defect Eng. Semicond. Technol. (GADEST '97),* Spa, Belgium: Balaban Publishers, 1997, pp. 115–120.
214. S. A. McHugo et al., Efficiency-limiting defects in polycrystalline silicon, in *1994 IEEE 1st World Conf. Photovoltaic Energy Convers.,* Waikoloa, HI: IEEE, Vol. 2, 1994, pp. 1607–1610.
215. H. Hieslmair et al., External gettering comparison and structural characterization of single and polycrystalline silicon, in *Defect Impurity Eng. Semicond. Devices,* San Francisco, CA: Materials Research Society, 1995.
216. K. Mahfoud et al., P/Al co-gettering effectiveness in various polycrystalline silicon, *Sol. Energy Mater. Sol. Cells,* **46**: 123–131, 1997.
217. H. Baker, *ASM Int.,* **3**: 1992.
218. P. Villars et al., *ASM Int.,* **3**: 1995.
219. M. Apel et al., Aluminum gettering of cobalt in silicon, *J. Appl. Phys.,* **76**: 4432–4433, 1994.
220. T. M. Buck et al., Gettering rates of various fast-diffusing metal impurities at ion-damaged layers in silicon, *Appl. Phys. Lett.,* **21**: 485, 1972.
221. T. Kuroi et al., Proximity gettering of heavy metals by high-energy ion implantation, *Jpn. J. Appl. Phys.,* **32**: 303, 1993.
222. J. Wong-Leung et al., Proximity gettering of Au to ion beam induced defects in silicon, *Nucl. Instrum. Methods B,* **96**: 253–256, 1995.
223. H. Wong et al., Gettering of gold and copper with implanted carbon in silicon, *Appl. Phys. Lett.,* **52**: 889–891, 1988.
224. H. Wong et al., Proximity gettering with mega-electron-volt carbon and oxygen implantations, *Appl. Phys. Lett.,* **52**: 1023–1025, 1988.
225. H. Wong et al., Impurity gettering by implanted carbon in silicon, in *Ion Beam Process. Adv. Electron. Mater.,* Materials Research Society, Vol. 147, 1989, pp. 97–106.
226. W. Skorupa et al., Carrier lifetime increase in silicon by gettering with a MeV-implanted carbon-rich layer, *Electron. Lett.,* **26**: 1898, 1990.
227. W. Skorupa et al., Iron gettering and doping in silicon due to MeV carbon implantation, *Nucl. Instrum. Methods B,* **74**: 70–74, 1993.
228. M. H. F. Overwijk et al., Proximity gettering of transition metals in silicon by ion implantation, *Nucl. Instrum. Methods B,* **96**: 257–260, 1995.
229. J. L. Benton et al., Iron gettering mechanisms in silicon, *J. Appl. Phys.,* **80**: 3275, 1996.
230. S. M. Myers et al., Gettering of Metal Impurities by Cavities in Silicon, in *Semicond. Silicon, 7th Int. Symp. Silicon Mater. Sci. Technol.,* H. R. Huff et al. (eds.), The Electrochemical Society, 1994, pp. 808–819.
231. V. Raineri et al., Gettering of metals by He induced voids in silicon, *Nucl. Instrum. Methods B,* **96**: 249–252, 1995.
232. S. M. Myers et al., Binding of cobalt and iron to cavities in silicon, *J. Appl. Phys.,* **80**: 3717, 1996.
233. S. A. McHugo et al., Competitive gettering of Cu in CZ silicon by implantation-induced cavities and internal gettering sites, *Appl. Phys. Lett.,* **69**: 3060–3062, 1996.
234. S. M. Myers and D. M. Follstaedt, Interaction of copper with cavities in silicon, *J. Appl. Phys.,* **79**: 1337–1350, 1996.
235. S. A. McHugo et al., Gettering of iron to implantation induced cavities and oxygen precipitates in silicon, *J. Electrochem. Soc.,* **145**: 1400–1405, 1998.
236. S. M. Myers and G. A. Petersen, Transport and reactions of gold in silicon containing cavities, *Phys. Rev. B,* **57**: 7015, 1998.
237. J. Wong-Leung et al., Gettering of Au to dislocations and cavities in silicon, *Appl. Phys. Lett.,* **67**: 416–418, 1995.

238. S. M. Myers et al., Solute binding at void surfaces in silicon and germanium, in *Mater. Res. Soc. Meet., Microcryst. Semicond.: Mater. Sci. Devices,* Vol. 283, 1993, pp. 549–554.

239. P. A. Stolk et al., The mechanism of iron gettering in boron-doped silicon, *Appl. Phys. Lett.,* **68**: 51–53, 1995.

240. T. A. Baginski, Back-side Germanium Ion Implantation Gettering of Silicon, *J. Electrochem. Soc.,* **135**: 1842, 1988.

241. C. J. Barbero et al., The gettering of copper by keV implantation of germanium into silicon, *J. Appl. Phys.,* **78**: 3012–3014, 1995.

242. F. Namavar et al., Gettering of impurities during high dose implantation of Al or Cr into Si and the resulting effect on structure and composition, in *Mater. Res. Soc. Meet., Impurity Diffus. Gettering Silicon,* Vol. 36, 1985, p. 55.

243. C. Griffioen et al., Helium desorption/permeation from bubbles in silicon: a novel method of void formation, *Nucl. Instrum. Methods B,* **27**: 417, 1987.

244. R. Liefting et al., Improved Device Performance by Multistep or Carbon Co-Implants, *IEEE Trans. Electron Devices,* **41**: 50–55, 1994.

245. P. A. Stolk et al., Implantation and transient boron diffusion: the role of the silicon self-interstitial, *Nucl. Instrum. Methods B,* **96**: 187, 1995.

246. J. P. d. Souza et al., Enhanced damage accumulation in carbon implanted silicon, *Appl. Phys. Lett.,* **64**: 3596, 1994.

247. L. W. Song et al., Bistable interstitial-carbon-substitional-carbon pair in silicon, *Phys. Rev. B,* **42**: 5765, 1990.

248. X. Lu et al., Ion-cut silicon-on-insulator fabrication with plasma immersion ion implantation, *Appl. Phys. Lett.,* **71**: 2767, 1997.

249. W. F. Ames, *Numerical Methods for Partial Differential Equations,* New York: Academic Press, 1977.

250. G. J. Reece, *Microcomputer Modelling by Finite Differences,* Basingstoke: Macmillan, 1986.

251. W. J. Minkowycz, *Handbook of Numerical Heat Transfer,* New York: Wiley, 1988.

252. D. Greenspan and V. Casulli, *Numerical Analysis for Applied Mathematics, Science, and Engineering,* Redwood City, CA: Addison-Wesley Pub. Co. Advanced Book Program, 1988.

253. F. M. Livingston et al., An infrared and neutron scattering analysis of the precipitation of oxygen in dislocation-free silicon, *J. Phys. C: Solid State Phys.,* **17**: 6253, 1984.

254. H. Hieslmair et al., Evaluation of precipitate densities and cature radii from the analysis of precipitation kinetics, *J. Appl. Phys.,* **84**: 713, 1998.

255. T. Y. Tan et al., Physical and Numerical Modeling of Impurity Gettering in Silicon, in *NREL/SNL Photovoltaics Program Review,* Lakewood, CO: AIP Conference Proceedings, 1996, p. 215.

256. T. Y. Tan et al., Diffusion-Segregation Equation and Simulation of the Diffusion-Segregation Phenomena, in *Semiconductor Silicon,* H. R. Huff et al. (eds.), San Francisco, CA: Electrochemical Society, 1994, p. 920.

257. D. A. Antoniadis and R. W. Dutton, Models for Computer Simulation of Complete IC Fabrication Process, *IEEE J. Solid-State Circuits,* **SC-14**: 412–422, 1979.

S. A. McHugo
Lawrence Berkeley National Laboratories

H. Hieslmair
University of California